SEMMELWEIS EGYETEM

DOKTORI ISKOLA

Ph.D. értekezések

3528.

JÁNOSKA ÁDÁM

A gyógyszerészeti tudományok korszerű kutatási irányai

című program

Programvezető: Dr. Antal István, egyetemi tanár

Témavezető: Dr. Tóth Gergő, egyetemi docens

TYROSINE KINASE INHIBITORS: PHYSICOCHEMICAL CHARACTERIZATION, CYCLODEXTRIN COMPLEXATION, AND PROTONATION-STATE-DEPENDENT RECEPTOR BINDING

PhD thesis

Ádám Jánoska

Semmelweis University Doctoral College

Pharmaceutical Sciences and Health Technologies Division





Supervisor:	Gergő Tóth, Ph.D.
Official reviewers:	Ida Fejős, Ph.D. Attila Almási, Ph.D.

Head of the Complex Examination Committee:	Zoltán Benyó, D.Sc.
Members of the Complex Examination Committee:	Szabolcs Béni, D.Sc. Ákos Urai, Ph.D.

Budapest
2026

TABLE OF CONTENTS

LIST OF ABBREVIATIONS 4

1 Introduction 6

1.1 Challenges in the development of cancer treatment 6

1.2 Protein-kinases 7

1.3 Growth factor receptor (GFR) as a therapeutic target 8

1.4 Studied tyrosine kinase inhibitors 8

1.4.1 Erlotinib 10

1.4.2 Lapatinib 11

1.4.3 Gefitinib 11

1.4.4 Vandetanib 12

1.5 Key aspects of the structure-activity relationships of tyrosine kinase inhibitors 13

1.6 Methods used to determine physico-chemical properties 14

1.6.1 Methods used to determine acid-base dissociation constants 14

1.6.2 Determination of lipophilicity 20

1.6.3 Determination of solubility 21

1.7 Cyclodextrins 22

1.7.1 Use and pharmaceutical relevance of cyclodextrins 23

1.7.2 Methods for equilibrium and structural characterization of cyclodextrin complexes 25

2 Objectives 29

3 Methods 30

3.1 Materials 30

3.2 Methods 31

3.2.1 Potentiometric titration 31

3.2.2 UV-pH titration 31
3.2.3 *Intrinsic* solubility determined by the Chasing Equilibrium Solubility method 32
3.2.4 Determination of partition coefficient using shake-flask method .. 33
3.2.5 Measurements by NMR 34
3.2.6 Determination of the stoichiometry of inclusion complexes using UV and NMR spectroscopy 35
3.2.7 Phase-solubility study 36
3.2.8 Molecular Modelling Study 36
4 Results 38
4.1 Physico-chemical properties 38
4.1.1 Potentiometric titration of erlotinib in methanol/water mixture 38
4.1.2 UV-pH titration of erlotinib and lapatinib 39
4.1.3 ^{1}H NMR-pH titration of erlotinib, vandetanib and gefitinib 40
4.1.4 Molecular modelling of the different protonation states regarding studied TKIs 41
4.1.5 Determination of lipophilicity 45
4.1.6 Determination of solubility 45
4.2 Interaction studies with cyclodextrins 45
4.2.1 Determination of stoichiometry of guest molecule-CD complex using the Job plot method 46
4.2.2 Determination of the apparent stability constants and solubility enhancement using phase-solubility tests 47
4.2.3 2D ROESY NMR spectroscopy studies 49
4.2.4 Molecular modelling 51
4.2.5 Study of tyrosine kinase receptor binding of TKIs 53
5 Discussion 55

5.1 Physico-chemical characterization of the studied tyrosine kinase inhibitors 55
5.2 Characterization of cyclodextrin complexation of TKIs 59
5.3 Evaluation of interactions with the binding domain of tyrosine kinase 62
6 Conclusions 64
7 Summary 65
8 References 66
9 Bibliography of the candidate's publications 78
9.1 Publication relevant to the dissertation 78
9.2 Other, not related publications 78
10 Acknowledgements 79

LIST OF ABBREVIATIONS

ATP	-	Adenosine triphosphate
BCRP	-	Breast Cancer Resistance Protein
CD	-	Cyclodextrin
CPMC	-	Conductor-like Polarizable Continuum Model
DS	-	Degree of substitution
DMSO	-	Dimethyl-sulfoxide
EGFR	-	Epidermal growth factor receptor
EMA	-	European Medicines Agency
FDA	-	U.S. Food and Drug Administration
GFR	-	Growth factor receptor
HER	-	Human epidermal growth factor receptor
HH	-	Henderson-Hasselbach
HP-β-CD	-	Hydroxypropyl-β-cyclodextrin
MS	-	Mass spectrometry
NMR	-	Nuclear magnetic resonance
NSCLC	-	Non-small cell lung cancer
OATP	-	Organic Anion Transporting Polypeptide
RAMEB	-	Randomly Methylated β-cyclodextrin
RET	-	Rearranged during transfection
ROESY	-	Rotating frame Overhauser Enhancement Spectroscopy
SBE-β-CD	-	Sulfobutylether-β-cyclodextrin
TKI	-	Tyrosine kinase inhibitor

UV	-	Ultraviolet
VEGFR	-	Vascular endothelial growth factor receptor

1 INTRODUCTION

1.1 Challenges in the development of cancer treatment

Cancer is one of the leading causes of death worldwide. Chemotherapy has been the primary therapy of choice for the last few decades. However, the drugs used for chemotherapy have a low therapeutic index and serious side effects [1]. For this reason, one of the most important tasks of medical and pharmaceutical research is the complete clarification of the pathomechanism of these diseases and the development of a suitable therapy. According to current knowledge, the formation of malignant tumor cells is the result of a multi-stage process which can be described as a series of genomic changes or the improper functioning of the intercellular communication system. Pharmaceutical research is currently focused on the development of drugs that act on specific signaling mechanisms relevant to the development and progression of malignant tumors.

With the help of active tyrosine kinase inhibitors (TKIs) already on the market (even in monotherapy), the complete eradication of certain cancers can be achieved (e.g. imatinib against chronic myeloid leukemia), and they can significantly increase the chance of survival in many serious cancer cases. The importance of TKIs is well illustrated by the fact that, in recent years, most small molecules approved by the FDA have come from this compound class. Their detailed characterization and improved understanding contribute to the development of new, safer cancer therapies.

The pharmacokinetics of ionizable drugs are strongly shaped by the properties of biological compartments—most notably pH, but also dielectric constant, temperature, and related factors. A molecular-level understanding of disposition and effect therefore requires rigorous physicochemical profiling of the active substances, including their protonation constants, solubility, and lipophilicity. Achieving the desired therapeutic outcome depends as much on appropriate pharmacokinetic behavior as on favorable pharmacodynamics. Membrane permeation is generally greatest for the unionized species, which typically exhibits the lowest aqueous solubility—highlighting the intrinsic trade-off between permeability and solubility. However, it should be noted that ionization state is an important parameter for the protein binding as well. The clinical application of TKIs is often hindered by their poor aqueous solubility. Solubility can be enhanced by several formulation strategies, including complexation with cyclodextrins (CDs). CDs are

widely used in the pharmaceutical industry to increase the solubility of hydrophobic compounds. They have been proven to have biocompatibility and beneficial toxicological properties, and the expansion of their pharmaceutical application and their positioning are still subjects of cutting-edge research. In the following chapters, I will introduce protein kinases, the molecules under investigation, and the methods employed throughout my PhD work.

1.2 Protein-kinases

In the molecular mechanism of the response of cells to external stimuli, the reversible phosphorylation of proteins plays a fundamental role, which are catalyzed by protein kinases in the intracellular space [2,3].

The functioning of these enzymes is influenced by the mediators found in the cells, which are either only involved in the given signaling pathway, and as a result, the protein kinase regulated by the given mediator is directly responsible for the effect or non-specifically has a role in changing the mechanism of the given protein phosphorylation. Chemical signals with receptors located in the plasma membrane either activate the given signal pathway with the help of the above-mentioned mediator, or without the intervention of a mediator, the chemical signal-receptor complex activates it directly by protein phosphorylation. There is a “crosstalk” between the activated signal pathways, which are completely different from each other, and the molecular basis of this information exchange is also mediated by proteins [4].

Proteins are phosphorylated on specific amino acid side chains by moving the γ-position phosphate group of adenosine triphosphate (ATP) to the specific OH-groups. Protein kinases are grouped according to whether they create a phosphate ester bond on a serine or threonine side chain (serine/threonine kinases), or they phosphorylate the OH-group of a tyrosine side chain (tyrosine kinases). The structure of protein kinases is characterized by a certain degree of similarity despite the differences in their function, regulation, and substrates. In the part of the enzymes responsible for catalysis, there is a characteristic, short, rich in glycine amino acid sequence followed by a lysine in the appropriate position, which is responsible for ATP binding [5]. Protein kinases can

recognize the often very basic or acidic amino acids located next to the side chain to be phosphorylated; thus, they can perform the phosphorylation of many different proteins.

In most cases the catalytic activity of protein kinases is strictly regulated. Protein kinases are found in almost all biochemical processes, such as regulation of growth and differentiation, metabolic pathways or regulation of cell reproduction. Kinases can be regulated both allosterically and by phosphorylation. Research has traced the causes of many diseases to improper functioning in signaling processes: cancer, chronic inflammatory processes, the development of diabetes, etc. It is therefore important to learn more about protein kinases, as these results can open new horizons in today's drug research [6,7].

1.3 Growth factor receptor (GFR) as a therapeutic target

Tyrosine kinase proteins play a key role in cell reproduction, but their abnormal functioning leads to serious diseases. In the last 20 years, countless families of tyrosine kinase enzymes have been identified, which are involved in the transduction of extracellular signals or are modulators located intracellularly. Our expanding knowledge of the structural and functional background of the growth factor receptor tyrosine kinase enzyme family and its role in the development of cancer has contributed to the research of new, specific target components in the GFR signaling pathway.

The research results showed that disruption of both the extracellular ligand-binding region of the receptor and the intracellular tyrosine kinase region in the signaling system increases the risk of cancer disease [8]. New potential anti-tumor drugs that target the external ligand-binding domain include several monoclonal antibodies, immunotoxins, and cytotoxic agents. Currently, the most promising chemotherapy drugs with GFR inhibitory function used in the clinic incorporate quinazoline and pyrazolo-pyrrolo-pyridopyrimidine structures.

1.4 Studied tyrosine kinase inhibitors

The studied TKIs in our work represent a class of small molecule inhibitors designed to interfere with the ATP-binding sites of tyrosine kinases, a family of enzymes critical to the regulation of signal transduction processes and, consequently, cellular

growth and division. The specificity of these inhibitors for kinases is grounded in the molecular structures of both the enzymes themselves and the inhibitors, which are engineered to exploit differences in the kinase domains.

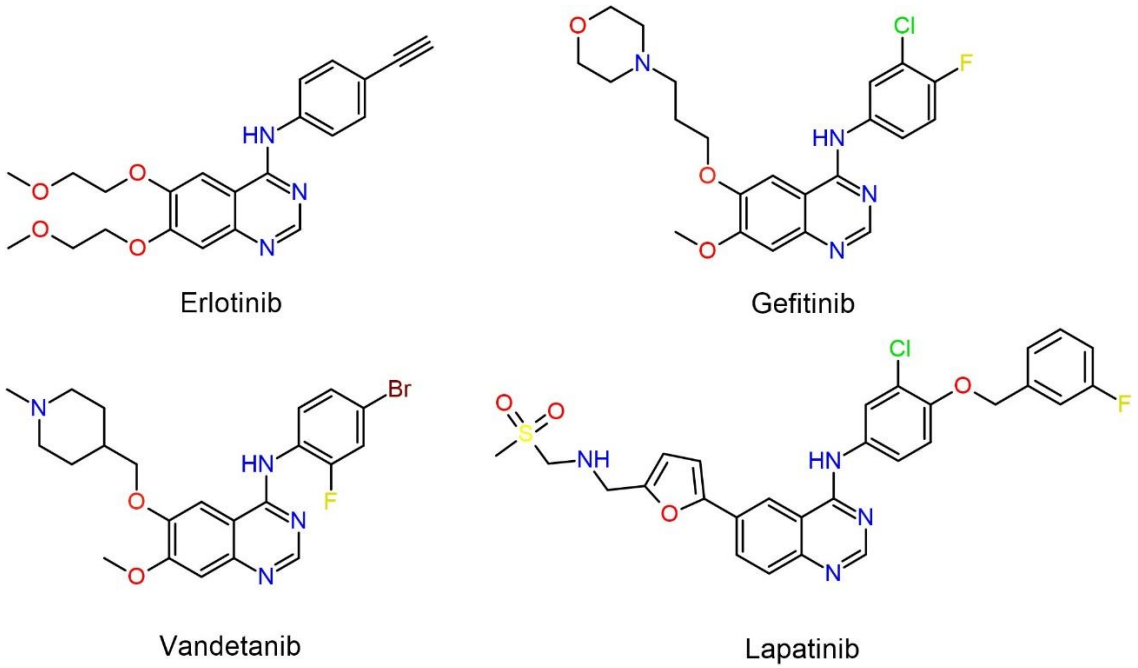


Figure 1.1. – Molecular structures of studied TKIs: erlotinib, gefitinib, lapatinib [9].

Erlotinib, gefitinib, and lapatinib have been primarily associated with the inhibition of the human epidermal growth factor receptor (HER) family, which includes EGFR and HER2/neu. These receptors are frequently overexpressed or mutated in malignancies such as NSCLC and breast cancer, making them prime targets for therapeutic intervention. Erlotinib and gefitinib have garnered attention due to their effectiveness in treating NSCLC patients with specific EGFR mutations, and lapatinib's dual-action against EGFR and HER2 has proven beneficial for patients with HER2-positive breast cancer.

Vandetanib, on the other hand, extends the scope of tyrosine kinase inhibition beyond the HER family by also targeting the vascular endothelial growth factor receptor (VEGFR) and RET tyrosine kinase. This broadened target profile is particularly pertinent in the context of medullary thyroid cancer, where these pathways play a significant role in disease progression.

Collectively, the choice to study these four TKIs is justified by their illustrative roles in the emerging field of molecularly targeted therapy. Their development and clinical application have provided invaluable insights into the treatment of various cancers and have set precedents for the design of new inhibitors. By examining these agents, researchers can continue to elucidate the complexities of tyrosine kinase signaling in oncogenesis, refine therapeutic strategies to overcome resistance mechanisms, and advance the overarching goal of precision medicine.

Below, we detail the TKIs evaluated in this work:

1.4.1 Erlotinib

Erlotinib, IUPAC chemical name: N-(3-ethynylphenyl)-6,7-bis(2-methoxyethoxy) quinazolin-4-amine (see *Figure 1.1*), selectively inhibits the intracellular tyrosine kinase domain of the epidermal growth factor receptor, by reversibly binding to the ATP binding site.

According to clinical studies, erlotinib has significant antitumor activity both in monotherapy and in combination with other agents. It can reduce the tyrosine kinase activity of HER1/EGFR to 50% (IC_{50}) at a concentration of 2 nM (0.8 ng/ml). Abnormal function of the HER/EGFR receptor leads to the development of several epithelial derived tumors, including NSCLC and pancreatic cancer [10]. In a clinical phase III study, the survival rate of patients with already treated and advanced NSCLC was significantly increased [11]. When erlotinib is combined with gemcitabine, a significant therapeutic effect can be achieved in locally advanced or already metastatic pancreatic cancer [12]. Based on these data, it is used as a second- and third-line treatment approved by the EMA and FDA in the form of 25, 100 and 125 mg film-coated tablets (Tarceva®).

After oral administration, the absorption of erlotinib is relatively rapid, reaching its peak plasma concentration in 4 hours. According to a study on healthy volunteers, the absolute bioavailability of the active ingredient is 59% [13]. Exposure after an oral dose may be increased by food. After absorption, at clinically relevant concentration conditions, 95% of erlotinib is bound to plasma proteins, mainly to albumin and α1-acid glycoprotein. Its volume of distribution is 232 L, which indicates significant tissue

distribution. The equilibrium blood level is reached in 7-8 days, its terminal elimination half-life is 36 hours [13,14].

1.4.2 Lapatinib

Overactivity of the epidermal growth factor receptor (ErbB1) and human epidermal growth factor receptor 2 (ErbB2) tyrosine kinase subfamilies have been associated with many breast, head and neck cancer diseases [15–17]. Lapatinib belonging to the 4-anilinoquinazoline group (chemical name: N-[3-chloro-4-[(3-fluorophenyl)methoxy]phenyl]-6-[5-[(2methylsulfonylethylamino)methyl]-2-furyl]-quinazoline-4 -amine) is a selective and reversible inhibitor of ErbB1 and ErbB2 tyrosine kinase.

The active ingredient is marketed under the name Tykerb® as a ditosylate salt in the form of a 250 mg film-coated tablet. Clinical trials showed that even lapatinib used as monotherapy caused a significant increase in the survival rate in previously untreated breast cancer patients. The bioavailability of lapatinib was less than 25%, and the AUC curve shows a high standard deviation [18]. Due to its absorption, the daily dose of the active ingredient is extremely high 1.0-1.5 g. The serum concentration appears in the blood after a delay of 15 minutes, reaching its peak concentration after 4 hours. At a daily dose of 1250 mg, reaching the equilibrium blood level, the plasma concentration is 2.43 μg/ml (coefficient of variation 76%). Taking the active ingredient together with a high-fat meal can result in an increase in bioavailability [19].

Lapatinib is strongly bound to plasma proteins (> 99%), mainly to albumin and α1-acid glycoprotein, like erlotinib. In vitro research has shown that lapatinib is a substrate of BCRP (ABCG1) and p-glycoprotein (ABCB1) transporters and can inhibit these efflux transporters and the hepatic OATP 1B1 transporter, which can be a source of interactions when other drugs are used. With a single daily dose, the equilibrium plasma concentration is reached after 6-7 days, with a plasma half-life of 24 hours.

1.4.3 Gefitinib

Gefitinib is the first selective inhibitor of epidermal growth factor receptor's (EGFR) tyrosine kinase domain. Chemical name: N-(3-chloro-4-fluorophenyl)-7-

methoxy-6-(3-morpholin-4-ylpropoxy)quinazolin-4-amine, marketed under the name of Iressa®. EGFR activating mutations have an important role in blocking apoptosis, increasing angiogenic factors and facilitating metastasis. Gefitinib is highly effective in non-small cell lung cancers with a mutation in the EGFR tyrosine kinase domain regulating anti-apoptotic pathways [20]. Clinical trials showed no activity without any EGFR mutation.

Marketed in 250 mg dose, administered as a single daily dose, peak plasma concentration reached relatively slowly between 3 to 7 hours after oral administration. The mean absolute bioavailability was found 59% in cancer patients and has no significant relation with nutrition [21]. Plasma protein binding is approximately 90%, binds to albumin and α1-acid glycoprotein. Gefitinib has an extensive distribution into tissue with a volume of 1400 L, resulting in a pharmacokinetic profile, which supports a once-daily dosage regimen [22].

1.4.4 Vandetanib

Vandetanib has proven activity against different epidermal growth factor receptor family like vascular endothelial growth factor (VEGF) receptors, RET, protein tyrosine kinase 6 (BRK), tyrosine kinase with immunoglobulin and EGF domains-2 (TIE2), members of the ephrin (EPH) receptor kinase family, and members of the Src family of tyrosine kinases [23]. Vandetanib contains the same 4-anilinoquinazoline structure, typical of TKIs (Chemical name: N-(4-bromo-2-fluorophenyl)-6-methoxy-7-[(1-methylpiperidin-4-yl)methoxy]quinazolin-4-amine).

Vandetanib is administered orally from 100 mg to 300 mg dose once a day, after administration peak plasma concentration achieved at a median of 6 hours, range 4-10 hours. For bioavailability, no data were available, presumably due to variable absorption and bioavailability for individual patients. During studies absorption was not significantly affected by the presence of food, approximately 69% was recovered with 44% in feces and 25% in urine [24]. Vandetanib binds to human serum albumin and alpha-1-acid-glycoprotein with *in vitro* protein binding being approximately 90%.

1.5 Key aspects of the structure-activity relationships of tyrosine kinase inhibitors

The structure-activity relationship (SAR) of TKIs refers to the relationship between the chemical structure of these compounds and their biological activity in inhibiting tyrosine kinases. This relationship helps in optimizing TKIs for better selectivity, potency, and pharmacokinetic properties. Nowadays there are many TKIs on the market or in the development phase. Some of them bind more kinases, and act as non-selective kinase inhibitors. Some developed selective TKIs like tovarafenib only inhibit RAF. Both approaches could have advantages and disadvantages as well. However, the structure activity relationship may change as a function of the target. Kinase inhibitor molecules can be classified into two major groups based on their binding mode to the protein: reversible and irreversible inhibitors. Since proteins primarily use ATP as an intracellular energy source, most reversible inhibitor molecules exert their effect at the enzyme's ATP-binding site, either in the active or inactive state of the kinase. The hinge region is responsible for forming hydrogen bonds with the adenine moiety of ATP, which is essential for kinase activity.

Here I would like to summarize the main structural elements and their impact on the activity:

- **Core scaffolds:** Most TKIs have a heterocyclic core, such as quinazolines (in erlotinib, gefitinib, vandetanib, lapatinib etc.) pyrrolopyrimidines (avitinib), or indoles (alectinib), which mimic ATP and interact with the ATP-binding site of kinases.

- **Substituents in the core ring:** The presence of electron-donating or withdrawing groups in the core ring highly affects kinase binding activity, for example quinazoline derivatives with an anilino group (like erlotinib and gefitinib) enhance the interaction with the hinge region of EGFR. The following Figure 1.2 shows how the core and substituents in the core ring influence the activity in the case of disubstituted pyridopyrimidine.

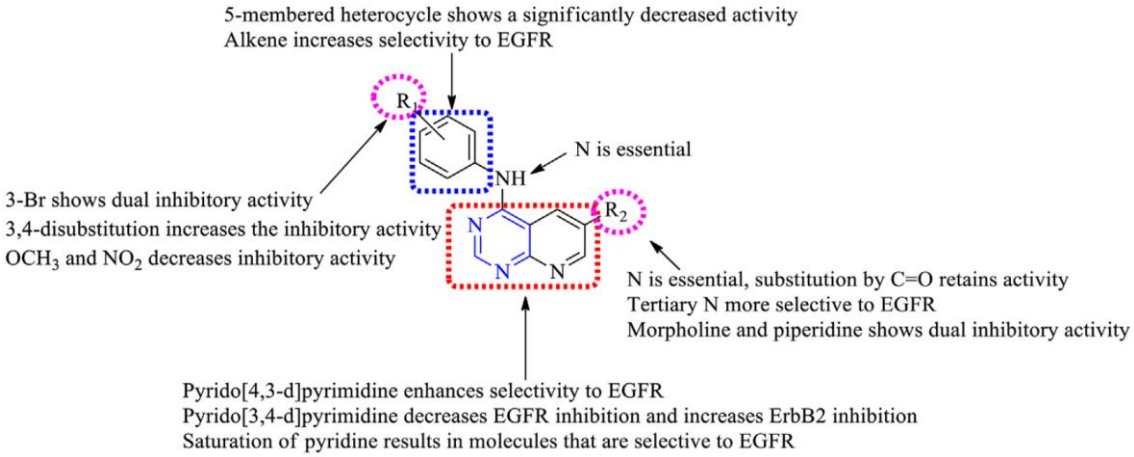


Figure 1.2 – Structure-activity relationship of tyrosine kinase inhibitors with pyridopyrimidine core [25]

In hinge-binding region, hydrogen bonding to key residues (e.g. Met793 in EGFR) is essential for strong inhibition. Alteration in linker groups (amide, ether, or sulfonamide) impact kinase specificity and selectivity. In the distal side chain region we can find the region that alters the physico-chemical properties and pharmacokinetics of the drug. Polar and ionizable groups in this region improve solubility and affect permeability. Some halogen atoms, for example fluorine substitution in lapatinib increases the metabolic stability.

1.6 Methods used to determine physico-chemical properties

1.6.1 Methods used to determine acid-base dissociation constants

Every analytical method is suitable for determining macroscopic protonation constants if the pH-dependent change of the measured physicochemical parameter can be clearly linked to the proton uptake of the molecule. Among the many methodologies, only those that were used in this thesis are reviewed below.

1.6.1.1 Potentiometric titration in aqueous medium

Since the publication of Jannik Bjerrum's dissertation, pH-potentiometric titration has been a classic, highly accurate method for determining protonation (and complex stability) constants [26,27]. Known volumes of a standard solution of a strong base are added to the solution of the compound to be tested (usually containing a known amount

of strong acid) while stirring. Taking the dilution into account, the concentration of the remaining unneutralized H^+ (OH^-) ions can be calculated for each point of the titration, and the concentration of free H^+ (OH^-) ions is measured through pH. Their difference gives the number of protons taken up by the ligand, as expressed by combining the stoichiometry for H^+ and L:

$$c_{H^+} - c_{OH^-} = [H^+] - [OH^-] + c_{L^z} \cdot \overline{n}_H \quad (1.1)$$

The limits of the pH-potentiometric titration can also be read from the equation above. The total concentration must be chosen in a way that the contribution of the H^+ absorption of the ligand is dominant on the right side of the equation (1.1), this is usually achieved in the pH range of 1.7-12.0. However, when measuring pK_a in a strongly acidic (or alkaline) medium, most of all H^+ (or OH^-) ions are freely present and the buffering capacity of the solution is not dominated by the ligand, but by the solvent [27]. This can be compensated by a ligand concentration greater than the usual 0.5-10 mM concentration, but then it is more difficult to keep the ionic strength at a constant value. To measure constants in the extreme pH range, it is more appropriate to choose the NMR-pH or UV-pH titration method [28]. Another disadvantage of pH potentiometry is that it is only suitable for testing highly pure and non-volatile substances. The contribution of impurities, possible stereoisomers or degradation products $c \cdot \overline{n}_H$ that ionize in the tested pH range cannot be separated from the substance to be measured in equation (1.1), which is the basis of the evaluation, they give a common buffer range(s) [27]. In situations, the interference of carbonate from atmospheric CO_2 complicates the measurement in the case of a ligand concentration of less than 1 mM, which can be prevented by introducing an inert gas (N_2 or argon) into or over the solution. During the evaluation of potentiometric titrations, the unknown protonation constants are determined so that the weighted sum of squares of the deviation of the calculated and measured mV values is minimal.

The measured titration curve can be directly transformed into the Bjerrum function by rearranging the balance equation (1.2):

$$\overline{n}H = \frac{c_{H^+} - c_{OH^-} - [H^+] + K_v[H^+]^{-1}}{c_{L^z}} \quad (1.2)$$

It is immediately clear from $\overline{n}_H = f(p[H])$ representation that, for example if a non-stoichiometric amount of strong acid is introduced together with a compound crystallized from an acidic solution, or the crystal water content is unknown, than c_{L^z} does not match the nominal value [29]. In such cases, for the unbiased estimation of the protonation constants, it is also necessary to recalculate the total concentrations from the derivative of the titration curve or based on equivalence point(s) calculated from Gran's linearization [30,31].

1.6.1.2 Potentiometric titration in an aqueous-organic co-solvent

One of the conditions for determining the pK_a of a compound by potentiometric titration is that the solubility of the compound should be at least $5 \cdot 10^{-4}$ M in the entire tested pH range [32]. In the case of poor solubility and a suitable chromophore group, the determination can be carried out by UV-pH titration, but in the absence of a suitable chromophore group, it is necessary to increase the solubility by adding an organic solvent component (cosolvent). The most often used is methanol [33], but dimethyl sulfoxide (DMSO), dimethylformamide, dioxane and acetonitrile can also be [34]. Mixtures of different cosolvents are prepared from water and the organic solvent, and the apparent p_sK_a value is determined by pH potentiometry in each solvent, and the value obtained by extrapolated to 100% water content, which cannot be directly measured in water [35].

Organic solvents can be classified according to protic/aprotic character, acidic/basic character, H-bond donor/acceptor character and polarity. In solvents (mixtures) with medium and high permittivity, the complete dissociation of strong electrolytes can be assumed with a good approximation, and to apply the electrode calibration and logK calculation methods to aqueous solutions, only the constant value of autoprotolysis needs to be modified [33,34].

1.6.1.3 Potentiometric titration in methanol-water mixtures

The combined glass electrode can be calibrated to the p_sH-scale [34] by blank titration, as in aqueous medium, if the Gran analysis confirms the complete dissociation of the strong acid and strong base in the solvent mixture. Compounds with similar structures are similarly solvated, therefore their protonation constants can be expressed

as a linear function of the $\log_w K$ basicity in an aqueous medium for any composition of a selected solvent mixture[36]:

$$log_s K = a_s \cdot log_w K + b_s \quad (1.3)$$

As the dielectric constant (ε_r) and organic solvent content of the mixtures change, the protonation constants also change and approach the value valid in water as the organic solvent content decreases. Yasuda and Shedlovsky's extrapolation formula (which also considers the decrease in water activity) gives a linear correlation for most compounds,

$$log_s K + log[H_2O] = a \cdot \frac{1}{\varepsilon_r} + b \quad (1.4)$$

thus, it can be obtained by linear extrapolation valid for the aqueous medium [33,34,37–39]. The slope *a* is positive when negatively charged groups are protonated, and negative or close to zero when neutral groups are protonated. This can even help in deciding which of several overlapping protonable groups has the greatest contribution to a given macroconstant.

1.6.1.4 NMR-pH titration

The chemical shift δ measured in ppm of an NMR active nucleus is defined by the following equation [40]:

$$\delta = \frac{v - v_{ref}}{v_0} \cdot 10^6 [ppm] = \frac{\sigma_{ref} - \sigma}{1 - \sigma_{ref}} \cong \sigma_{ref} - \sigma \quad (1.5)$$

where v is the resonance frequency [Hz] of the selected nucleus and v_{ref} is the frequency of the reference materials nucleus, σ and σ_{ref} are the shielding factors for the same nuclei, and ν_0 is the base frequency [MHz] of the used spectrometer for the nucleus being measured. As a result of protonation, the electron density around the functional group decreases, which is decreasing the diamagnetic shielding of the nearby NMR nuclei, therefore the chemical shift changes. Since most small molecules exchange protons at a rate close to the diffusion limit in water, these reactions are instantaneously fast on the "chemical shift" time scale (fast-exchange regime): $k >> |v_L - v_{HL}|$, where v_L and v_{HL} are the frequencies of the examined NMR nucleus in the transforming L and HL axiparticle species. In this case, only one common resonance signal can be observed in

the mole fraction-weighted average of the individual chemical shifts δ_L and δ_{HL} of the particles[41]:

$$\delta^{measured} = \delta_L x_L + \delta_{HL} x_{HL} = \frac{\delta_L + \delta_{HL} K[H^+]}{1 + K[H^+]} \quad (1.6)$$

Upon protonation of a ligand capable of accepting *n* number of protons, the chemical shift of a selected nucleus in its pH function is given by the following equation:

$$\delta^{measured} = \delta_L x_L + \delta_{HL} x_{HL} + \cdots + \delta_{H_nL} x_{H_nL} = \sum_{i=0}^{n} \delta_{H_nL} x_{H_nL} = \frac{1}{\alpha_H} \sum_{i=0}^{n} \delta_{H_nL} \beta_{H_nL} [H^+]^i \quad (1.7)$$

By measuring the chemical shift of *K* number of NMR-active nuclei at a pH value of *M*, a data matrix of size *M* x *K* is obtained, which, gives the logβ (or log$K$) macroconstants and the unique chemical shift ($\delta_{H_iL_{m,k}}$) of the H_iL particles for each measured nuclei. From the perspective of statistical thermodynamics, α_H corresponds to the partition function of the grand canonical ensemble (also known as the "binding polynomial").

As the field strength of the superconducting magnets increases, the precision with which chemical shifts can be measured improves [42], so the accuracy of the calculated log$K$ is increasingly determined by the precision of the pH measurement (± 0.02).

Many forms of performing NMR pH-titration are known, of which we present the technique used in this thesis. In the traditional single-sample NMR titration, the titration solution is added in µl increments to a single NMR tube and the pH is measured with a microelectrode in the tube inaccurately without any adequate mixing. During single-sample NMR titration, it is preferable to determine the pH *in situ* with an indicator molecule present in the solution. From the measured chemical shift of the indicator, the pH can be calculated using the following equation (1.8),

$$pH = log\, K_{Ind} + \frac{\delta_{Ind}^{measured} - \delta_{HInd}}{\delta_{Ind} - \delta_{Ind}^{measured}} \quad (1.8)$$

if the limit shifts δ_{Ind} and δ_{HInd} and the value of log K_{Ind} are precisely known from a separate experiment. The accuracy of the pH obtained from equation (1.8) (via error propagation) is determined by the standard deviation of the chemical shifts, and pH can be calculated in the interval [logK_{Ind} - 1, logK_{Ind} + 1] with acceptable accuracy [43]. The

use of NMR indicators has long been widespread for in situ pH measurement of biological samples [44], however, Szakács et al. compiled a series of five indicators covering the entire range 0 < pH < 12 [43]. It was found that p[H] values between 0.0 and 1.8 can be determined with the dichloroacetic acid indicator without bias and with less random error than with a glass electrode [43]. For this, the protonation constant of dichloroacetate must be known precisely, for which a special NMR titration was also developed [28,41,45]. Another important aspect is the choice of a reference substance for NMR titration that does not change its ionization state in the tested pH range [46].

One of the advantages of NMR spectroscopic pK_a measurement is that it is not necessary to know the exact concentration of the substance to be measured, and possible impurities do not interfere, if the assignation of the resonance signals can be clearly determined and the substance to be tested does not interact or react with these impurities.

1.6.1.5 Optical spectroscopy titration

Nowadays, UV-pH titration can be considered a widely used method for determining pK_a. Ultraviolet-visible spectrophotometry can be used to determine pK_a if the ionizable group of a compound is located near the chromophore group and change in the pH causes a change in the spectrum corresponding to the protonation state of the ionizable group. UV-pH titration is the primarily used method to determine the dissociation constants of compounds whose low solubility does not allow the use of potentiometric titration. In such cases, depending on the specific absorption coefficient of the compound, we can even measure at a concentration two orders of magnitude lower (usually 50 μM).

During the measurement, a series of solutions with the same compound concentration and the same ionic strength, but with different pH, must be prepared, and the spectrum of each solution must be recorded. The dissociation constant of the compound can be calculated using the following equation:

$$A_{pH(\lambda)} = A_{L(\lambda)}x_L + A_{HL(\lambda)}\lambda x_H L = \frac{A_{L(\lambda)} + A_{HL(\lambda)}K[H^+]}{1+K[H^+]} \quad (1.9)$$

where A_{pH} is the absorbance value measured at the given pH, A_L and A_{HL} are the absorbance of the completely unprotonated and fully protonated particles at a given

wavelength, while x_L and x_{HL} are the mole fractions of the two particles. An appropriate wavelength (λ) should be selected where the difference in molar absorptivity between the two species is maximized. [47].

1.6.2 Determination of lipophilicity

Lipophilicity is one of the oldest and most widely used physicochemical parameters in drug research. For decades, log*P*—the logarithm of the octanol/water partition coefficient—was often the sole molecular descriptor employed in QSAR analyses (with log*D* later adopted to capture pH-dependent distribution). Today, there has been a move towards complex physico-chemical characterization, but the determination of log*P* is still essential in this process. Lipophilicity is the molecular property that most strongly determines the fate of a molecule in the body, both at the pharmacokinetic and pharmacodynamic (interaction with the receptor) stages, and is much more informative than a mere number, since it is formed by the same interactions that occur between the molecule and its biological environment.

Experimental determination of the partition coefficient often employs methodologies such as the shake-flask technique or reverse-phase high-performance liquid chromatography (RP-HPLC) [48]. Complementarily, two-phase chromatography, utilizing biphasic systems with immiscible aqueous and organic phases, enables the quantification of lipophilicity based on differential retention times. This chromatographic modality is particularly adept at mirroring the partitioning behavior of drug molecules within biological membranes [49]. In parallel, *in silico* modelling provides a theoretical framework for the prediction of lipophilicity, exploiting molecular descriptors to predict distribution trends without the need to rely on laboratory experiments [50].

In our study, the traditional shake-flask method was used for determining the partition coefficient. During the measurement, the aqueous and the immiscible organic phase (most commonly octanol) are pre-saturated with each other. This eliminates the error caused by dissolution. The substance to be tested is dissolved in the aqueous phase, its concentration is determined, and the organic phase is added. The two phases are brought into contact by vigorous shaking until equilibrium is reached. The solvents are then separated by centrifugation and the concentration of the substance in the two phases

is determined by an appropriate quantitative analytical method. For reasons of simplicity and accuracy, concentration is most often determined by spectrophotometry if the spectral properties of the substance under test conditions allow it. In special cases, the concentration can be measured by HPLC [51] or GC [52]. Accurate concentration measurement in octanol is difficult due to the unfavorable properties of octanol (e.g. high viscosity, volatility). However, according to Leo et al., it is not necessary to determine the concentration of the substance in octanol after representative control of the mass balance, but it is sufficient to measure the decrease in concentration of the aqueous phase [53]. Furthermore, the main sources of error in the shake flask technique (e.g. formation of emulsions or micelles during shaking, imperfect phase separation, errors due to impurities of the test sample or the solvents and reagents used) have been identified. The main aspects of validation of the shake-flask method have been published by Dearden and Bresnen [54].

The disadvantages of the method are that it is labor and time intensive, requires relatively large quantities of high purity material, it is difficult to thermostat and can only be used over a relatively narrow log*P* range. For compounds with log*P* values greater than +4 or less than -2, the distribution fraction cannot be determined with satisfactory accuracy by the shake-flask method. Due to the very low solubility of highly lipophilic or hydrophilic molecules in one of the partition phases, an extreme phase ratio must be used, which increases the measurement error [55]. Under validated conditions, the average error of the method is 0.05 - 0.10 log units in the log*P* range -2 to +3.

1.6.3 Determination of solubility

The biological, chemical and biochemical processes necessary for the body to function take place in an aqueous medium. The action of drugs therefore depends on their solubility in water. The aqueous compartments of the body provide a favorable environment for polar compounds; therefore, a certain degree of hydrophilicity is necessary for dissolution, distribution, and renal elimination. However, the passive permeation of biological membranes requires lipophilicity. Consequently, an ideal drug molecule exhibits a balanced combination of hydrophilic and lipophilic characteristics. However, it has been observed that the drug candidate molecules of the last decades have

an increasing molecular weight and an increasing lipophilicity. Accordingly, the hydrophilic property is decreasing or becoming less important, which may result in poor bioavailability [56].

The numerical value of thermodynamic (equilibrium) solubility gives the concentration of the solution phase of a heterogeneous two-component system in thermodynamic equilibrium. Its value is constant at a given pressure and temperature and is characteristic of the quality of the material. For ionizable molecules, solubility is pH dependent.

A method for solubility determination was developed based on potentiometric titration, this is the Chasing Equilibrium Solubility: CheqSol method [57]. This method has the advantage of being suitable for both equilibrium and kinetic solubility determination, requires low amount of material, it is fast, automated and reproducible. The method depends on the selection of a concentration at which precipitation occurs during the potentiometric titration. CheqSol has the disadvantage that it is only suitable for determining the solubility of ionizable compounds.

The measurement should be carried out in such way that the compound (organic acid or base) is present in the solution in ionized and dissolved form. During the titration, at the pH at which the neutral form of the compound predominates, the non-ionized form must precipitate, which is detected by the optical cable immersed in the solution. To measure solubility, it is therefore essential to provide a quantity of material at which the compound is still completely dissolved at the pH corresponding to its ionized form but precipitates out of solution at the pH of its neutral form. For the measurement, the substance to be measured is dissolved in a known volume of an aqueous solution of an inert salt (usually 0.15 M KCl). The instrument mixes the sample throughout the experiment and measures the pH of the solution. The volume and concentration of the sample solution is continuously recorded by instrument control software.

1.7 Cyclodextrins

CDs are cyclic, non-reducing oligosaccharides built up from D-glucopyranose units via α-(1,4)-glycosidic linkages. The individual CDs are named according to the number of glucose units they contain, so that in the case of 6, 7 and 8 units, respectively,

we distinguish between α-, β- and γ-CDs. The glucopyranose units that make up CDs are arranged on the surface of a truncated cone. The inner cavity of the molecule is relatively apolar due to the orientation of C–H bonds and glycosidic oxygen atoms. The narrower opening of the truncated cone is lined with primary hydroxyl groups, while the wider opening is bounded by secondary hydroxyl groups. Due to the high polarity of the rim hydroxyl groups, CDs are highly soluble in water (except β-CD). The schematic structure of CDs is shown in Figure 1.3 [58,59].

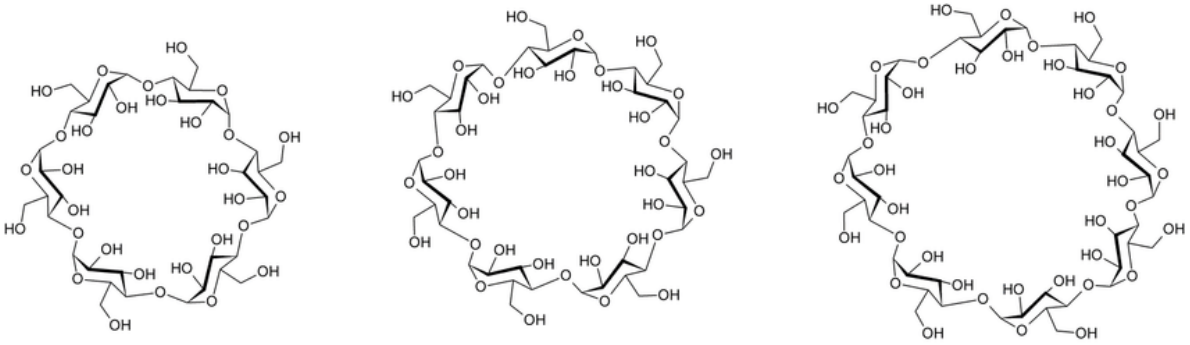


Figure 1.3 - Structural scheme of native α-, β- and γ-cyclodextrins composed of D-glucopyranose units

The CDs contain one primary and two secondary hydroxyl groups per glucose unit (a total of 18, 21 and 24 free OH groups for α-, β- and γ-CD, respectively), which provide an excellent opportunity to prepare a wide variety of derivatives. For CD derivatives, the degree of substitution is defined as the average number of hydroxyl groups substituted per molecule. Today, the number of CD derivatives described in the literature is more than a thousand. In general, CD derivatives can be classified in two ways: according to the number of substituents and their ionizability. In the former case, we are talking about monofunctional (degree of substitution = 1), multifunctional random (degree of substitution between 1 and 21 for β-CD) or isomerically pure (degree of substitution is an integer) derivatives. Introducing an ionizable substituent imparts either a permanent or a pH-dependent charge to the CD.

1.7.1 Use and pharmaceutical relevance of cyclodextrins

Nowadays CDs are widely used, given the variety of derivatives and diverse applications. Today, thousands of tons of CDs are used in industry. RAMEB is used in

the paint industry to produce water-based paints and wood staining solutions, while HP-β-CD is used in cleaning and cosmetic products. In the food industry, CDs used as food additives stabilize flavors and volatile compounds, reduce unwanted tastes and odors, and improve product shelf-life. CDs and their derivatives are utilized in analytical chemistry, mainly in the field of chromatographic techniques owing to their chiral recognition ability [60].

In the pharmaceutical industry, CDs and their derivatives are used for the molecular encapsulation of poorly water-soluble active substances to enhance their solubility and bioavailability, to stabilize formulations of volatile active substances, and to counteract local irritation of the active substance. There are currently dozens of preparations on the market in which the active substance is in an inclusion complex of CD. Pharmaceutical forms containing CD cover almost the entire spectrum, including registered tablets, capsules, oral solutions, nasal sprays, suppositories, creams, ointments, infusions, injections, nail lacquers and eye drops [60–63]. A recent publication shows that more than 120 active pharmaceutical ingredients on the market are formulated with CDs. Numerous medicinal products contain various CD derivatives, with β-CD and its modified forms being the most widely used. Among the derivatives applied in approved formulations, hydroxypropyl derivatives of β- and γ-CDs, sulfobutyl-ether-β-CD, randomly methylated β-CD, and sulfolipo-β-CD are the most common. There are already innovative TKIs with hydroxypropylated CD, such as larotrectinib and quizartinib, offering targeted therapies for patient with specific genetic alterations in tropomyosin receptor kinase fusion cancers and fms-like tyrosine kinase 3 mutated acute myeloid leukemia, respectively [64]. Table 1. shows examples of marketed CD formulations:

Table 1. Examples of approved pharmaceutical formulations with native cyclodextrin and cyclodextrin derivatives

Drug	CD	Trade Name	Dosage form	Company
Remdesivir	SBE-β-CD	Veklury	i.v.	Gilead Sciences
Voriconazole	SBE-β-CD	Vfend	i.v. solution	Pfizer
Posaconazole	SBE-β-CD	Noxafil	i.v. solution	Merck
Itraconazole	HP-β-CD	Sporanox	oral solution	Janssen

Quizartinib	HP-β-CD	Vanflyta	i.v.	Daiichi Sankyo
Larotrectinib	HP-β-CD	Vitrakvi	capsules, oral solutions	Bayer
Nitroglycerin	β-CD	Nitropen	sublingual tablet	Nippon Kayaku
Olmesartan medoxomil	β-CD	Olmetec OD Tablets	OD tablet	Daiichi Sankyo
Omeprazol	β-CD	Omebeta	enteric capsule	Betafarm, Stada
Cetirizine	β-CD	Zyrtec, WalZyr, Revicet	chewing tablet,OD tablet,dry syrup	Losan Pharma, UCB Pharma, Sandoz, Walgreen, Sawai Pharm., Nichi-Iko, Takeda

For a long time, it was thought that the bioavailability of CD-containing formulations was poor due to the slow release of the active substance from the CD cavity, but Stella et al. have shown that both the rate of formation and dissociation of the drug/CD complex are generally diffusion controlled [65]. Consequently, a water-soluble drug/CD complex at the surface of hydrated epithelial cells can significantly increase the bioavailability of a highly lipophilic, poorly water-soluble drug, but can also cause a decrease in bioavailability for a drug with good water solubility and permeability [66].

1.7.2 Methods for equilibrium and structural characterization of cyclodextrin complexes

The formation of a supramolecular complex in the equilibrium reaction of a ligand L (guest molecule) and CD, and the thermodynamic constant characterizing the stability of the complex, are illustrated in equation 1.10 [67]:

$$iL + jCD \leftrightarrow CD_jL_i \qquad K_{CD_jL_i} = \frac{[CD_jL_i]}{[L]^i[CD]^j} \tag{1.10}$$

The stoichiometry of the inclusion complex is defined by the coefficients *i* and *j*. The simplest and most common is a complex consisting of one CD and one guest

molecule, but a 1:2 stoichiometry is also relatively common. Examples of highly diverse compositions can also be found in the literature [67].

There are stoichiometric and thermodynamic conditions for the formation of the inclusion complex. For a CD to partially or completely incorporate the guest molecule without covalent bonding, by purely intermolecular forces, the basic criterion is a proper sterical fit, i.e. the ability of part or all of the guest molecule to enter and fit into the CD cavity. The internal diameter, and consequently the cavity volume, limits the range of guest molecules that can be accommodated by the CD. The other criterion is the presence of a sufficiently favorable free-enthalpy difference between the hydrated reactants (L and CD) and the resulting complex(es). In aqueous solution, the slightly apolar CD cavity is occupied by energetically unfavorable, highly ordered water molecules. As a result of the unfavorable polar-apolar interaction, replacement by a less polar guest molecule is thermodynamically favored. In an aqueous medium, two thermodynamic processes favor complex formation: the release of cavity water, which subsequently forms numerous hydrogen bonds in the bulk solvent, and the associated gain in enthalpy and entropy upon displacement of these energetically constrained water molecules. At the same time, there is a loss of interactions between the hydrophobic guest molecule and the polar solvent, followed by the formation of secondary interactions between the apolar cavity of the CD and the hydrophobic guest, including mainly van der Waals, hydrophobic interactions and hydrogen bonds.

Methods for the quantitative characterization of the stability of CD complexes are those in which the change in the measured physico-chemical quantity can be clearly related to complex formation. In the following, we summarize only those methodologies that have been applied in the present work.

1.7.2.1 Ultraviolet-visible spectrophotometry

The most widely used method is the phase-solubility assay developed by Higuchi and Connors [68], which spectrophotometrically measures the increase in solubility after equilibrating an excess amount of the guest molecule in solutions containing increasing concentrations of CD. By plotting the total (typically submillimolar) concentration of the guest molecule as a function of the CD concentration, the resulting function provides

information on the stoichiometry of the complex formed and even the stability constant can be calculated from the slope and intercept of the plot. The advantage of the method is that the intercept also provides the intrinsic solubility of the guest molecule in solvent not containing CD.

1.7.2.2 NMR spectroscopy

NMR spectroscopy is one of the most versatile techniques for the solution-phase equilibrium and structural characterization of CD complexes [69]. The study of CDs and their complexes started in the second half of the 1960s [70,71], also due to the increasing performance of spectrometers. Among the first NMR results, the hydrogen bond structure formed between the secondary hydroxyl groups of various native CDs was published, which helped to explain the extremely low solubility (0.013 M) of β-CD [72,73]. The ^{1}H and ^{13}C chemical shifts of CDs were determined from early studies, their spin systems and conformational changes analyzed, and with the advent of 400 MHz and higher field devices and gradient techniques, it became possible to study various substituted CDs and their complexes [74].

NMR shift titration is the most used method for the equilibrium characterization of the CD-guest molecule system. Usually, the chemical shift change (Δδ) is measured on one or more NMR active nuclei of the guest molecule upon addition of increasing amounts of CD. The complex stability constant is obtained from the Δδ vs. CD concentration dataset by nonlinear parameter fitting [67,75].

To accurately determine the stability constant, titration should be carried out between 0-80% complex formation grade if the solubility data allow. The chemical shifts measured in ^{1}H (less frequently ^{13}C) spectra taken at different host/guest concentration ratios represent the mole-fraction weighted average of the individual $\delta_{H_nI^{n+}}$ and $\delta_{H_nI^{n+}-CD}$ chemical shifts of the particles, if the complexation reaction is sufficiently fast on the NMR time scale:

$$\delta^{measured} = \delta_{H_iI^{i+}} \cdot x_{H_iI^{i+}} + \delta_{H_iI^{i+}-CD} \cdot x_{H_iI^{i+}-CD} = \frac{\delta_{H_iI^{i+}} + \delta_{H_iI^{i+}-CD} \cdot K_{H_iI^{i+}-CD}[CD]}{1 + K_{H_iI^{i+}-CD}[CD]} \qquad (1.11)$$

The advantage of NMR titration is that the effect of complex formation on all NMR spin-active nuclei of both the guest molecule and the CD can be monitored simultaneously, so that several data sets are available for *K* determination from a single titration. An additional advantage of the method is the extent to which the apparent stability constants diverge when the chemical shift changes measured on each nucleus are evaluated separately. If the resulting stability constants differ by more than 10% or exhibit a systematic trend, an additional equilibrium process must be incorporated into the assumed 1:1 stoichiometric model - most commonly a 2:1 complex - when evaluating the weighted averages [76,77].

NMR pulse sequences make it possible to investigate the three-dimensional structures of supramolecules. The intramolecular cross-peaks observed in two-dimensional Nuclear Overhauser Effect Spectroscopy (NOESY) provide valuable information for signal assignment and for determining the conformations of non-symmetric CD derivatives. The applicability of conventional NOE methods is strongly influenced by the correlation motion of molecules. The critical cross-relaxation times depend on both the solvent viscosity, the rotational correlation time (τ_c) and the spectrometer frequency. On a 500-600 MHz instrument, a positive NOE (fast motion, $\varpi\tau_c << 1$) is expected for compounds below 1000 Da, while a negative NOE ($\varpi\tau_c >> 1$) is expected only for compounds with molecular weights well above 5000 Da. CDs and their complexes typically fall within an intermediate correlation-time regime ($\varpi\tau_c \approx 1$), which makes NOESY generally unsuitable for these systems. In rotating-frame Overhauser effect spectroscopy (ROESY), a spin-lock field is applied during the mixing time, causing cross-relaxation to occur not along the z-axis but along an effective axis with x–y components. Because this occurs at an effective frequency (ϖ_{eff}) distinct from the spectrometer's Larmor frequency, the condition $\varpi\tau_c \ll 1$ is satisfied for virtually any molecular rotational rate. As a result, ROESY spectra exhibit cross-peaks that are opposite in phase to the diagonal [78,79].

2 OBJECTIVES

The overall aim of this PhD work was to obtain a comprehensive physicochemical characterization of selected TKIs and to explore how their fundamental molecular properties influence solubility, complex formation, and protonation-dependent behavior in biological systems.

To achieve this, the specific objectives were:

1. To determine the acid–base properties (pK_a values) of the selected TKIs and describe their protonation equilibria in aqueous solution, establishing the speciation patterns relevant under physiological conditions.
2. To characterize the aqueous solubility and lipophilicity profiles of each compound and evaluate how ionization state influences these properties.
3. To investigate whether CD complexation can enhance the solubility of poorly water-soluble TKIs, and to determine the stoichiometry and stability of the corresponding inclusion complexes.
4. To characterize the structure and binding geometry of TKI–CD complexes, using solution-state methods to gain molecular-level insight into host–guest interactions.
5. To assess how protonation state, molecular conformation, and inclusion complexation influence the physicochemical behavior of the studied TKIs, with implications for formulation development and biopharmaceutical performance.

These objectives together support a deeper understanding of how fundamental molecular properties govern the solubility, complexation, and protonation-dependent behavior of TKIs, contributing to the rational design of improved drug formulations.

3 METHODS

3.1 Materials

All CDs α-, β-, γ-CD, HP-β-, RAMEB- and SB-β-CD were the products of Cyclolab R&D Ltd, Hungary. CDs and their most important properties are summarized in Table 2. TKIs (erlotinib, lapatinib, gefitinib and vandetanib) were purchased from Eurasia's Ltd, India. Tris(hydroxymethyl)aminomethane (Tris), H_3PO_4, KH_2PO_4, KOH, NaOH and HCl were of analytical grade from commercial suppliers. D_2O, DCl and n-octanol were obtained from Sigma-Aldrich, Hungary. HPLC-grade methanol (MeOH) and acetonitrile (ACN) were purchased from Merck, Germany. The deionized water was prepared by a Milli-Q Direct 8 Millipore system, France.

Table 2. Properties and abbreviations of used cyclodextrins

Cyclodextrin	Abbreviations	Substituent	Degree of substitution (DS)	Purity (%)	Molecular weight (g/mol)
α-cyclodextrin	α-CD	-	-	100	972.9
β- cyclodextrin	β-CD	-	-	100	1135.0
γ- cyclodextrin	γ-CD	-	-	100	1297.2
randomly methylated β- cyclodextrin	RAMEB	$–CH_3$	12	12	1303.4
hydroxylpropylated β-cyclodextrin	HP-β-CD	$–CH_2$-CH(OH)–CH_3	6.3	>98	1497.6
carboxymethylated β-cyclodextrin	CM-β-CD	$CH_2–COO^-$	3.5	>95	1375.1
sulfobutylated β-cyclodextrin	SB-β-CD	$(CH_2)_4SO_3^-$	6	>95	2084.2

3.2 Methods

3.2.1 Potentiometric titration

The protonation constant (pK_a) of erlotinib was determined by pH-potentiometric method as follows. A combined Ag/AgCl glass electrode coupled to a GLpKa analyser was used for titration. The electrode was calibrated in aqueous medium in methanol/water mixture using the so-called four-parameter calibration procedure (Four Plus™ method) [80]. Due to the poor water solubility of erlotinib, the log$K$ value was determined by the co-solvent method. The apparent ionization constants (logK') in the medium were determined in methanol/water mixtures with different proportions of organic solvents ranging from 31-49 wt%. Titrations were performed under nitrogen gas at constant ionic strength (I = 0.15 M KCl) and temperature (t = 25.0 ± 0.5 °C). For each measurement, 6 mL of 1 mM erlotinib solution was prepared, acidified to pH = 2 with 0.5 M HCl solution and titrated to pH = 10 with 0.5 M KOH solution. Log$K$' values were calculated from 3 parallel measurements using the RefinementPro™ program.

The log$K$' values measured in the given methanol/water mixture were then extrapolated to the aqueous medium (zero methanol concentration) using the Yasuda-Shedlovsky method [39]. According to this method, there is an inverse relationship between the log$K$' value and the dielectric constant of the solvent mixture:

$$log\ K' + log[H_2O] = a/\varepsilon + b \qquad (3.1)$$

where ε is the dielectric constant and log[H_2O] is the logarithm of the molar concentration of water in the given methanol-water mixture.

3.2.2 UV-pH titration

The protonation constants of erlotinib and lapatinib were determined using a D-PAS spectrophotometer (Sirius Analytical Instruments Ltd., UK) coupled to a GLpKa autotitrator. During the measurement, a spectrophotometer was directly connected to the titrator, and an optical cable was extended into the titration vessel, allowing spectra to be recorded after each titrant addition throughout the titration [81].

A stock solution of 6 mM in methanol was prepared for the measurement of erlotinib. Aliquots of the stock solution (100 µl - 150 µl) were transferred into 15 mL sample vessels containing 0.15 M KCl solution to achieve a final concentration of 40–60 µM. For each measurement, the sample solution was acidified to pH = 2 with 0.5 M HCl solution and titrated to pH = 10 with 0.5 M KOH solution. The spectra of the samples were recorded in the wavelength range between 200 and 700 nm. About 20 pH measurements and absorption spectra were obtained from each titration.

Titrations were performed under nitrogen gas at constant ionic strength (I = 0.15 M KCl) and temperature (t = 25.0 ± 0.5 °C). The pK_a and p$_s K_a$ values were calculated from three parallel measurements using the RefinementPro^{TM} program.

For lapatinib, UV–pH titration could not be performed in purely aqueous solution due to its low water solubility. Therefore, the co-solvent-based approach described in section 3.2.1 was applied. The apparent acid-base constants were measured in six different solvent mixtures ranging from 23-43 wt% methanol content. Titrations were performed under nitrogen gas at constant ionic strength (I = 0.15 M KCl) and temperature (t = 25.0 ± 0.5 °C). Stock solutions of 20 µM concentration were prepared and UV spectra were recorded at 19 different pH values. RefinementPro^{TM} was used to evaluate the results, calculated from three replicates.

3.2.3 *Intrinsic* solubility determined by the Chasing Equilibrium Solubility method

The thermodynamic solubility of neutral bases was measured using the Chasing Equilibrium Solubility (CheqSol) technique [82]. Solubility was monitored using an optical fiber connected to a GLpKa titration device, with the absorbance changes recorded by a D-PAS spectrophotometer. The operation of the instrument was managed by RefinementPro^{TM} and CheqSol software from Sirius, Forest Row, UK. The titration process was carried out in a nitrogen atmosphere at a controlled temperature of 25.0 ± 0.5 °C, utilizing solutions of 0.5 M HCl and 0.5 M KOH. For each measurement, three replicates were conducted.

The measurement was carried out by weighing a certain amount of the active substance into titration vessels and dissolving it in 10 ml of a 0.15 M KCl solution. A certain amount of acid was added to the basic solutions to ensure a pH value at which the compounds were present in the solution in fully protonated form. Aliquots of the KOH

solution were added to the solution of the ionized molecule until the solution became turbid. The precipitation of the base with poor water solubility from the solution was monitored by a spectrophotometer. In this two-phase system, small pH changes were induced by adding acid or base, causing the concentration of the neutral species to oscillate around their equilibrium saturation level. These pH perturbations triggered processes that transiently produced either undersaturated or supersaturated conditions in the solution. The exact pH value at which the system would be in equilibrium can be determined from the changes in the pH gradient, from which the thermodynamic solubility of the non-ionized particle can be calculated based on mass and charge equilibria [57].

3.2.4 Determination of partition coefficient using shake-flask method

The shake-flask method was used to determine the partition coefficient. To minimize errors due to mutual solubilization, the water and immiscible octanol layers were pre-saturated with one another for a duration of 24 hours. The compounds studied were dissolved in the aqueous phase, and their concentrations were determined prior to addition of the octanol phase. For all compounds except lapatinib, the pH of the aqueous phase was adjusted to pH 11 using NaOH. Following phase combination, the systems were agitated for 12 hours to ensure equilibration. This duration was sufficient for the establishment of partition equilibrium, while no detectable degradation of the compounds was observed under these conditions. After equilibration, the phases were separated by centrifugation [53]. The concentration of the substances in the aqueous phase was measured both before and after the equilibrium using a Jasco V-550 diode array UV spectrophotometer at a wavelength of 250 nm. The log*P* value was determined by UV-spectrophotometry according to equation:

$$log\ P = log(\frac{A_0 - A_1}{A_1} R) \quad (3.2)$$

where A_0 and A_1 are absorbances of water phase before and after partition, and R is phase ratio.

The partition coefficient (log*P*) could not be measured directly due to the high log *P* value of lapatinib. Therefore, the distribution coefficient (log*D*) was determined at acidic pH (pH = 2), where the molecule exists in a dicationic form, as well as at two

additional pH values (pH 5.83 and 6.11). Three parallel measurements were performed at each pH. The pH was measured using a Metrohm 6.0204.100 combined glass electrode connected to a Metrohm 780 pH meter. The water/n-octanol phase ratio ranged between 250 and 600. The log$P$ values of the individual macrospecies were calculated using the following equation:

$$D_{pH} = \chi_i P_i = \chi_{LAP^{2+}} P^{LAP^{2+}} * \chi_{LAP^{+}} P^{LAP^{+}} * \chi_{LAP} P^{LAP} \quad (3.3)$$

where χ is the mole fraction of the corresponding macrospecies, of the charge indicated.

3.2.5 Measurements by NMR

NMR spectroscopy measurements were carried out using a Varian Unity Inova DDR spectrometer with a frequency of 599.9 MHz for ^{1}H, equipped with a 5mm inverse detection z-gradient probe (IDPFG). The data from these measurements were analysed using VNMRJ 2.2C/Chempack 4.0 software package.

3.2.5.1 ^{1}H NMR-pH titration

Studied TKIs (erlotinib, gefitinib and vandetanib) were accurately weighed to prepare a 1 mM solution, to which 0.2 mM of DSS was added as an internal reference standard. NMR-pH titration of lapatinib could not be performed because the substance precipitated during the measurement. The titration experiments were executed at a maintained ionic strength of 1.0 M KCl, at a temperature of 25 °C in a solvent system composed of 5% D_2O and 95% H_2O. 1H NMR spectra were recorded using solvent suppression by the double pulsed field gradient spin echo (dpfgse) sequence was employed [83]. The pH measurements were conducted in a 5 ml solution under continuous mixing, and 600 µl of this solution was subsequently loaded into an NMR tube. The pH measurements were carried out using a Metrohm 6.0234.110 combined glass electrode, except where the pH was below 2.0. To avoid glass electrode error, dichloroacetic acid was used as an in-situ NMR pH indicator molecule below pH < 2.0. The pH was determined based on the chemical shift of the NMR indicator molecule, as described by equation (1.8), which incorporates the indicator's protonation constant (K_{ind} with a value of 1.14 for dichloroacetic acid) and the chemical shift values of the indicator

(δ_{ind} = 6.050, δ_{Hind} = 6.345 for dichloroacetic acid) [28]. The pK_a values were determined from the chemical shift-pH curves by non-linear parameter fitting using the OriginPro 8 software.

3.2.5.2 Analysis of the structure of inclusion complexes by 2D-ROESY NMR measurements

The position and orientation of the guest molecules within the inclusion complexes were investigated using phase-sensitive 2D ROESY NMR spectroscopy. The experimental solutions contained 2 mM native β-CD and 1 mM of the studied TKIs, dissolved in a solvent mixture of 30% DMSO and 70% D_2O. The pH level was set to 2.0 using a 30% DCl solution. The spectral data were acquired with a mixing time ranging from 300 to 500 milliseconds, across 64 scans and 512 data points for each 256 increments.

3.2.6 Determination of the stoichiometry of inclusion complexes using UV and NMR spectroscopy

UV spectroscopy measurements were performed using a Jasco V-550 diode array spectrophotometer, utilizing a quartz cuvette with a 10 mm path length at a constant temperature of 25 °C. NMR spectroscopy measurements were carried out as mentioned in chapter 3.2.5. The determination of the complex's stoichiometry was achieved by using Job's method of continuous variation [84]. Solutions with different [ligand]/[CD] ratios were prepared while keeping the sum of [ligand] + [CD] constant, and then the UV absorbance or chemical shift of the solutions was measured. The overall molar concentration was kept constant at 2.5 x 10^{-5} M during the experiment. Solutions were prepared with the molar ratio of the TKI and native β-CD molecules ranging from 0 to 1 (χ as molar ratio), after which the absorbance (A) or chemical shift (δ) of each solution was measured. The absorbance curves were obtained at the wavelength corresponding to the maximum change in absorbance (ΔA).

3.2.7 Phase-solubility study

The phase-solubility study for TKIs was conducted using the Higuchi and Connors method [68]. To the supersaturated solutions of the drug increasing amounts of native CD or their derivatives were added. The solutions were adjusted to pH 2 using HCl, and KCl was added to maintain an ionic strength of 0.15 M. After stirring these mixtures for 24 hours, they were left undisturbed to settle for an additional 24 hours. Following this, the concentration of the drug in the clear solutions was measured using UV spectrophotometry with a Jasco V-550 diode array spectrophotometer.

For a 1:1 complex formation, the stability constants of the complex can be calculated from the phase solubility diagram (TKI concentration vs CD concentration) as per the given equation (3.4).

$$K_{stab} = \frac{tg\alpha}{S_0(1-tg\alpha)} \quad (3.4)$$

In this equation, S_0 represents the drug's intrinsic solubility, which is indicated on the vertical axis, and $tg\alpha$ the slope of the linear part of the graph provides stability constant.

3.2.8 Molecular Modelling Study

Calculations were conducted using the Schrödinger suite (Released: 04-2020). The molecular structures of the four TKIs were generated using the Maestro graphical user interface (version 13.6.122). The LigPrep module refined these structures, utilizing the OPLS4 force field. Epik Classic and Epik 7 tools within the software suite estimated the potential protonation states across a pH range of 1.0 - 13.0. The most likely conformations of the TKIs were selected for subsequent molecular docking studies. Docking simulations used the inactive form of the EGFR tyrosine kinase domain (Protein Data Bank ID: 4HJO)[85]. The 4HJO protein structure was prepared using the Protein Preparation Wizard's default settings in the Schrödinger suite[86]. The protein's residue protonation states were estimated at a physiological pH using PROPKA [87], and the OPLS3e force field was applied during the minimization process [88]. The Receptor Grid Generation module defined the docking target region. Glide software performed the docking, utilizing flexible docking options and extra precision (XP) mode [89,90].

Additionally, the PM6 semi-empirical quantum chemistry method optimized the most likely protonation states of the inhibitors. These optimized structures, in complex with (β-CD), were compared for system stability. The Gaussian 16 program package was used to perform the calculations. The CPCM implicit solvent model, which approximates an aqueous environment (ε = 78.3553), and was applied to model solvent effects [91,92]. Thermodynamic properties derived from these calculations provided a basis for comparing the stability of the inclusion complexes.

4 RESULTS

4.1 Physico-chemical properties

4.1.1 Potentiometric titration of erlotinib in methanol/water mixture

The protonation constant (pK_a) of erlotinib was determined using UV–pH titration, ^{1}H NMR–pH titration, and pH-potentiometry. Using these three independent analytical methods, errors from individual titrations can be minimized and additional information on the protonation of the quinazoline ring can be obtained.

The co-solvent method was used to determine the protonation constant of compounds that are poorly soluble in water. The most widely used and studied organic solvent mixture is the methanol/water system, as methanol most closely mimics the solvation characteristics of water [33]. The apparent ionization constants (p$_s K_a$ values) were determined in different methanol/water mixtures and extrapolated to zero organic solvent content — that is, to aqueous solution — to obtain the true pK_a value [39]. The Yasuda–Shedlovsky extrapolation accounts for the decreased relative activity of water in mixed solvents; thus, a linear relationship is obtained by plotting the apparent dissociation constants against the reciprocal of the relative permittivity of the solvent mixtures (Figure 4.1). The extrapolated value was pK_a = 5.25 ± 0.02.

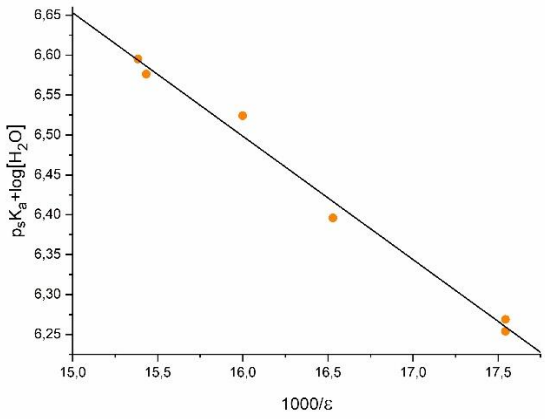


Figure 4.1 - Yasuda-Shedlovsky extrapolation for the determination of the protonation constant of erlotinib [93].

4.1.2 UV-pH titration of erlotinib and lapatinib

The pK_a value of erlotinib was also determined by UV-pH titration. Due to the high specific absorbance of the compound, titration was performed directly in aqueous solution. The protonable group of erlotinib is part of the UV chromophore, thus the spectrum during protonation is very sensitive in the 225-400 nm range. The obtained pK_a value was 5.39 ± 0.03.

The protonation constant of lapatinib was determined by UV-pH titration in methanol/water mixtures. A linear relationship between the apparent ionization constants (p$_s K_a$ values) and solvent composition was observed only up to 60 wt% methanol concentration. At higher methanol fractions, the p$_s K_a$–permittivity plot became sigmoidal, resulting in distorted extrapolation and therefore unusable data. For lapatinib, the solubility is so low that the base precipitates during the titration even in high-methanol solvent mixtures at appropriate stock solution concentrations. For pH-potentiometric or ^{1}H NMR-pH titrations therefore neither of them can be performed. The UV–pH titration followed the same solvent–composition strategy as described for potentiometry. In different solvent mixtures, apparent acid-base constants (p$_s K_a$) were determined. Because the protonable sites lie within or near the chromophoric regions, the protonation process can be monitored by UV spectroscopy. The obtained apparent ionization values were extrapolated to 0 wt% methanol content according to the Yasuda-Shedlovsky method (Figure 4.2.), yielding a value of 5.08 ± 0.05 for pK_{a1} and 7.72 ± 0.07 for pK_{a2}.

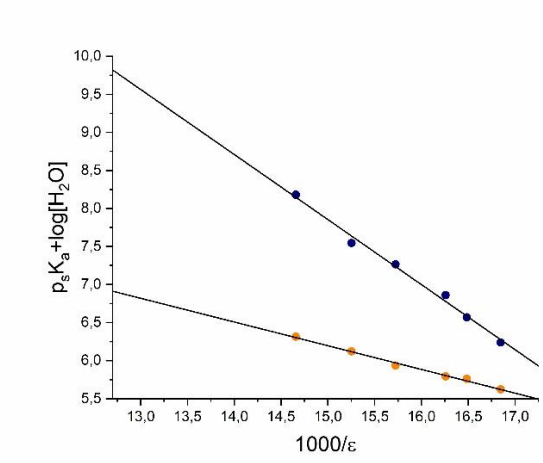


Figure 4.2 - Yasuda-Shedlovsky extrapolation to determine the protonation constants of lapatinib [94].

4.1.3 ^{1}H NMR-pH titration of erlotinib, vandetanib and gefitinib

To refine our estimation of the pK_a values and gain a deeper insight into the protonation mechanisms of the 4-anilinoquinazoline scaffold at the atomic scale, we conducted a detailed study using NMR-pH titration. The measurement was carried out as follows: solutions covering the pH range 0–12 were prepared, and the change in chemical shift as a function of pH was monitored for the carbon-bonded aromatic hydrogens H^2, H^5 and H^8 (hydrogens on the quinazoline ring) located closest to the protonation site.

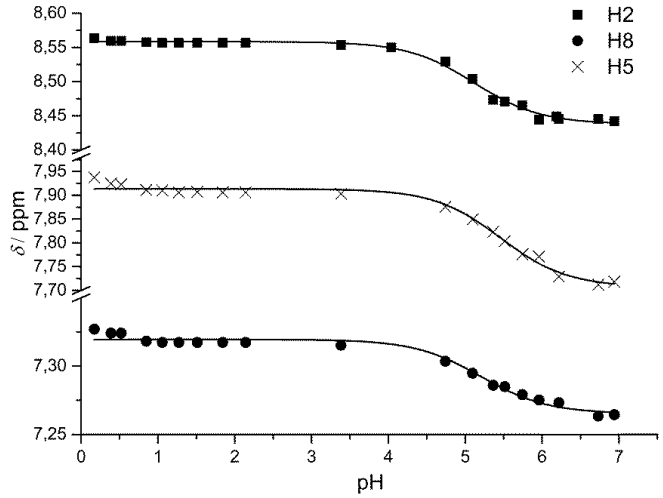


Figure 4.3 - Variation of chemical shift of specific carbon-bonded protons of erlotinib as a function of pH [93].

Gefitinib and vandetanib each have two protonation centers, whereas erlotinib can only be protonated on the quinazoline ring. The pK_a calculated for erlotinib from equation (1.6) is 5.32 ± 0.06, which shows a good correlation with pH-potentiometry and UV-pH measurements. In addition, the protonation values determined by ^{1}H NMR-pH titration for gefitinib are pK_{a1}=5.05 ± 0.02 and pK_{a2}=7.11 ± 0.02, while for vandetanib pK_{a1}=5.29 ± 0.08 and pK_{a2}=9.11 ± 0.02, by examining the chemical shifts of the aromatic hydrogens H2, H5 and H8.

4.1.4 Molecular modelling of the different protonation states regarding studied TKIs

For erlotinib, the Epik Classic algorithm identified six possible protonation states, whereas Epik 7 predicted only three. Taken together, the combined predictions yielded three neutral structures (erlotinib-01, -05, -06), two mono protonated forms (erlotinib-02, -03), and one anionic species (erlotinib-04), as shown in Table 3. Both prediction methods consistently identified erlotinib-01 to erlotinib-03. This subset includes one neutral structure (erlotinib-01) and two protonated variants in which either the N1 atom (erlotinib-02) or the N3 atom (erlotinib-03) of the quinazoline ring is protonated.

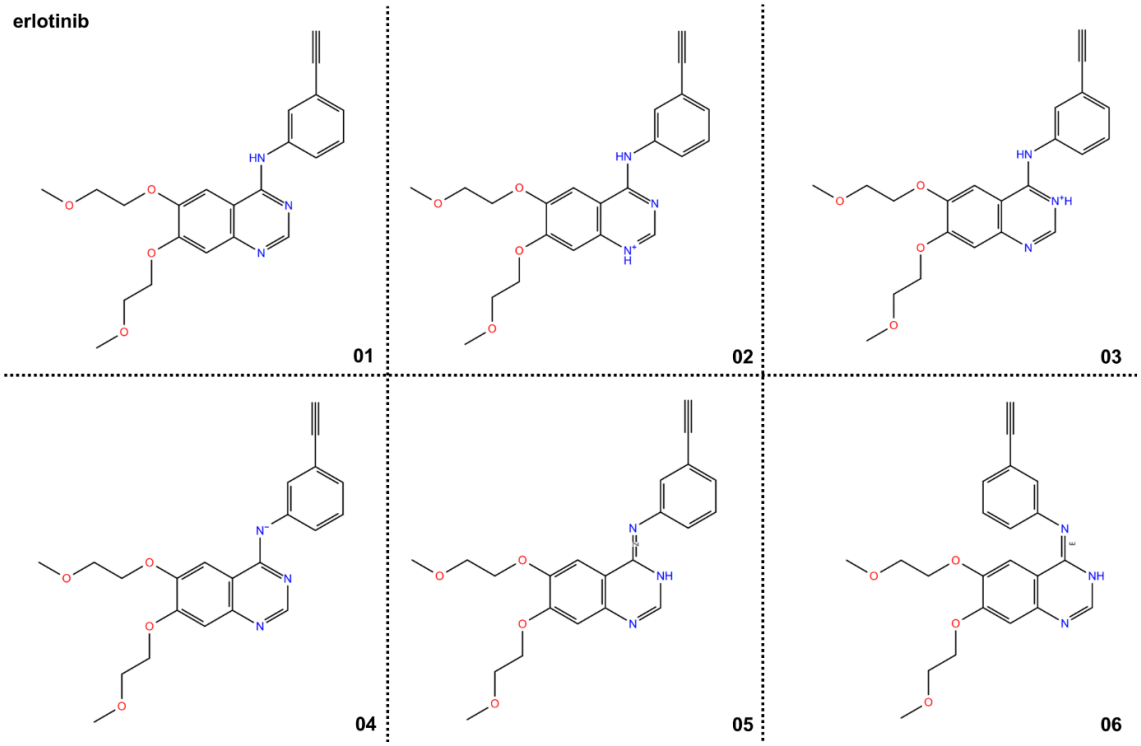


Figure 4.4 - All possible protonation states of erlotinib calculated by Epik 7 and Epik Classic

Table 3. State penalty values for all possible protonation states of erlotinib calculated by Epik 7 and Epik Classic - The numbering used in the table corresponds to the numbering used in Figure 4.4

Erlotinib	**Calculation of Epik Classic** / kcal/mol	**Calculation of Epik 7** / kcal/mol
ERL-01 – unprotonated	0.0015	0.0018
ERL-02 – N1 protonated	3.5729	3.4407
ERL-03 – N3 protonated	6.2483	5.9991
ERL-04 – 4-amine deprotonated	6.5137	-
ERL-05 – N3 protonated, cis 4-amine	7.4290	-
ERL-06 – N3 protonated, trans 4-amine	7.4290	-

Protonation states of lapatinib were also evaluated. In total, nine distinct microspecies were predicted: one neutral form, five monocationic forms (+1), two dicationic forms (+2), and one anionic form (−1) (Table 4.). Epik Classic identified eight possible states, whereas Epik 7 predicted seven (Table 4.). Six states—lapatinib-01 through lapatinib-05 and lapatinib-09—were common to both workflows. Among the shared species, three are monoprotonated (+1), arising either from protonation of the secondary amine adjacent to the sulfonyl group or from protonation of the quinazoline core.

Table 4. State penalty values for all possible protonation states of lapatinib calculated by Epik 7 and Epik Classic

Lapatinib	**Calculation of Epik Classic** / kcal/mol	**Calculation of Epik 7** / kcal/mol
LAP-01 – unprotonated	1.1014	0.0574
LAP-02 – secondary amine protonated	0.1043	1.4172
LAP -03 – N3 protonated	4.7781	4.2719
LAP -04 – N1 protonated	4.9263	6.2792
LAP -05 – sec. amine; N3 protonated	4.1627	7.6390
LAP -06 – sec. amine deprotonated	-	5.5446
LAP -07 – N3 protonated, trans 4-amine	7.3811	-

LAP -08 – N3 protonated, cis 4-amine	7.3432	-
LAP -09 – sec. amine; N1 protonated	3.2525	5.6317

A detailed evaluation of gefitinib indicated that ten distinct protonation states are feasible, comprising three neutral species, five monocationic species (+1), and two dicationic species (+2) (Table 5.). Epik Classic predicted all ten states, whereas Epik 7 identified six (gefitinib-01 to gefitinib-06). Thus, the six states predicted by Epik 7 were a subset of those generated by Epik Classic. Consistent with the observations for lapatinib, three of the shared species are monoprotonated (+1), arising from protonation either at the secondary amine of the morpholine moiety or at the quinazoline core. For the diprotonated gefitinib structures (gefitinib-05 and gefitinib-06), protonation occurs at both sites, i.e., on the quinazoline core and on the morpholine unit (Table 5.).

Table 5. State penalty values for all possible protonation states of gefitinib calculated by Epik 7 and Epik Classic

Gefitinib	**Calculation of Epik Classic** / kcal/mol	**Calculation of Epik 7** / kcal/mol
GEF-01 – unprotonated	0.4260	0.1735
GEF-02 – N1 protonated	4.1292	3.6305
GEF-03 – N3 protonated	6.3359	6.2496
GEF-04 – morpholin N protonated	0.3983	0.8190
GEF-05 – morpholin; N1 protonated	4.0126	4.2760
GEF-06 – morpholin; N3 protonated	6.4771	6.8951
GEF-07 – N3 protonated, cis 4-amine	7.1219	-
GEF-08 – N3 protonated, trans 4-amine	7.1219	-
GEF-09 – morpholin; N3 protonated, cis	7.1404	-
GEF-10 – morpholin; N3 protonated, trans	7.1332	-

The protonation behavior of vandetanib was also investigated. Eight distinct protonation states were predicted, comprising one neutral species, five monocationic species (+1), and two dicationic species (+2), mirroring the overall charge-state

distribution observed for gefitinib. Epik Classic identified all eight states, whereas Epik 7 proposed five (Table 5.). Notably, all five Epik 7 states (vandetanib-01 to vandetanib-05) were included among the Epik Classic predictions.

Among the Epik 7 set, two species are monoprotonated (+1), arising either from protonation of the quinazoline core or from protonation of the nitrogen atom of the N-methylpiperidine moiety. In the dicationic vandetanib structures (vandetanib-04 and vandetanib-05), both the quinazoline core and the N-methylpiperidine groups are protonated (Table 6.), consistent with the trends described for the other TKIs.

Table 6. State penalty values for all possible protonation states of vandetanib calculated by Epik 7 and Epik Classic

Vandetanib	**Calculation of Epik Classic** / kcal/mol	**Calculation of Epik 7** / kcal/mol
VAN-01 – unprotonated	3.6349	3.4530
VAN -02 – piperidine N protonated	0.0056	0.0033
VAN -03 – N1 protonated	6.7532	6.9813
VAN -04 – piperidine; N1 protonated	2.9457	3.5316
VAN -05 – piperidine; N3 protonated	4.7832	6.1853
VAN -06 – N3 protonated	7.9207	-
VAN -07 – N3 protonated, cis 4-amine	6.5383	-
VAN -08 – N3 protonated, trans 4-amine	6.5383	-

As the next step of the study, we aimed to determine which nitrogen atom in the 4-anilinoquinazoline scaffold exhibits the highest proton affinity. For this, the state penalties of the predicted protonation states were calculated using Epik Classic and Epik 7. The state penalty values associated with protonation on the quinazoline amino group in the para N1-position are predicted to be at least 2.00 kcal/mol lower in each TKI.

4.1.5 Determination of lipophilicity

To characterize lipophilicity, the partition coefficient (log*P*) of the fully unionized active compounds in the n-octanol/water system was determined. The results are shown in Table 7.

Table 7. Octanol/water partition coefficient of the investigated TKIs.

	Lipophilicity (log*P*)
Erlotinib	2.75 ± 0.02
Gefitinib	3.65 ± 0.08
Vandetanib	4.12 ± 0.13
Lapatinib	5.65 ± 0.25

4.1.6 Determination of solubility

The compounds we tested are in Class II of the Biopharmaceutical Classification System (BCS) which means that they have low solubility and high permeability. For the determination of intrinsic solubility CheqSol method was used, the results are shown in Table 8.

Table 8. Summarized solubility values of TKIs.

	Solubility (S_0)
Erlotinib	4.91 ± 0.9 μg/ml = 12.5 μM
Gefitinib	86.0 ± 2.53 μg/ml = 192.3 μM
Vandetanib	44.3 ± 0.13 μg/ml = 93.1 μM
Lapatinib	0.48 ± 0.12 ng/ml = 210.0 pM

4.2 Interaction studies with cyclodextrins

In the case of active substances with low solubility, various CDs can be successfully used to increase solubility, which may lead to an increase in bioavailability. In the experiments described below, the most suitable cavity size for complexation of CDs incorporating the guest molecule was identified and the variable complex stability

resulting from substitution of CDs was investigated. The complex stability values are important parameters, because if the stability value is too low, there will be no complex formation, whereas if the value is too high, the active substance will not dissociate from the complex and cannot exert a biological effect. In addition to stability, the stoichiometry and geometry of complexes have been investigated using various techniques.

4.2.1 Determination of stoichiometry of guest molecule-CD complex using the Job plot method

Job's continuous variations method was used to study the stoichiometry of ligand-CD complexes. The procedure is based on measuring the change in the concentration of the product by keeping the sum of the concentrations of the two reactants at a constant value but continuously varying their ratios. The variation of the physico-chemical parameters under study is maximized when the two reactants are present in exact stoichiometric proportions.

The calculated $\Delta A\chi$ and $\Delta\delta\chi$ values were plotted as a function of molar composition (χ). In all cases of the studied TKIs, the curves obtained showed a maximum for the solution with a molecular fraction of 0.5, indicating a 1:1 complex stoichiometry. Figures 4.5 and 4.6 show the Job plot curves for erlotinib β-CD and vandetanib β-CD, respectively.

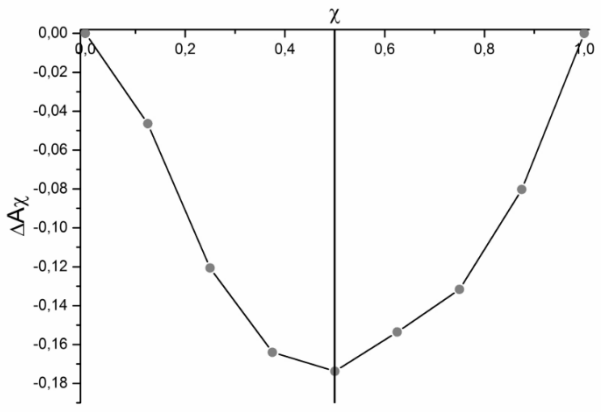


Figure 4.5 - Job plot curve for erlotinib-β-CD using UV spectroscopy [93]

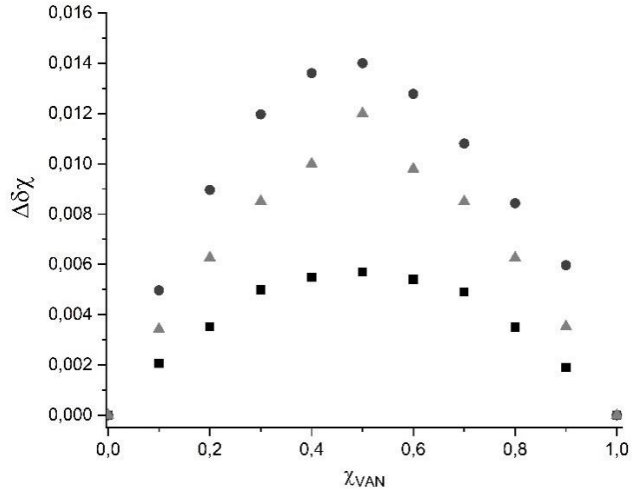


Figure 4.6 - Job plot curves for vandetanib-β-CD using NMR spectroscopy [9].

4.2.2 Determination of the apparent stability constants and solubility enhancement using phase-solubility tests

The increase in the solubility of the guest molecule is strongly dependent on the stability of the cyclodextrin inclusion complex, and therefore the determination of the stability constant of TKI-CD is very important [95].

The stability of the inclusion complexes formed between the studied TKIs and six CDs (α-CD, β-CD, γ-CD, HP-β-CD, RAMEB, and SBE-β-CD) at pH 2 was assessed using phase-solubility tests. Within the studied concentration range the phase-solubility profiles were linear (so-called A_L-type curve), which also demonstrates the 1:1 stoichiometry of the inclusion complex in all cases [68]. The stability constant of the CD complexes of TKIs with 1:1 stoichiometry was calculated from the phase-solubility diagram using equation (3.4). The resulting logK_{stab} values are shown in Table 9, the solubility enhancement at 10 mM CD is also calculated. Among the native CDs, β-CD formed the most stable inclusion complexes; therefore, further studies were performed with β-CD and its derivatives.

Table 9. The logarithm of the stability constants ($\log K_{stab}$) obtained from phase solubility studies and the solubility enhancement at 10 mM CD concentration [9].

	$\log K_{stab}$ (with solubility enhancement at a 10 mM CD concentration)			
CD	Erlotinib	Lapatinib	Vandetanib	Gefitinib
α-CD	2.15 ± 0.09 (2.3X)	1.66 ± 0.12 (1.4X)	1.34 ± 0.03 (1.2X)	1.49 ± 0.05 (1.3X)
β-CD	2.43 ± 0.05 (4.0X)	2.07 ± 0.11 (2.4X)	2.32 ± 0.05 (3.0X)	2.29 ± 0.01 (2.7X)
γ-CD	1.73 ± 0.05 (1.6X)	1.93 ± 0.09 (1.7X)	2.16 ± 0.02 (2.5X)	2.07 ± 0.07 (2.3X)
RAMEB	2.37 ± 0.08 (3.5X)	2.73 ± 0.04 (4.5X)	1.88 ± 0.07 (1.5X)	2.19 ± 0.04 (3.5X)
HP-β-CD	2.63 ± 0.11 (4.4X)	2.52 ± 0.03 (4.7X)	2.37 ± 0.12 (3.1X)	2.40 ± 0.11 (4.0X)
SBE-β-CD	3.37 ± 0.15 (23X)	4.33 ± 0.10 (183X)	3.18 ± 0.18 (17X)	3.51 ± 0.15 (34X)

4.2.3 2D ROESY NMR spectroscopy studies

2D ROESY NMR measurements were used to determine the structures of the assumed complexes at the atomic level. To investigate the structure of the TKI-β-CD complex, we recorded the ^{1}H NMR spectrum of each TKI. Figure 4.7. shows the ^{1}H NMR spectrum of lapatinib in acidic medium.

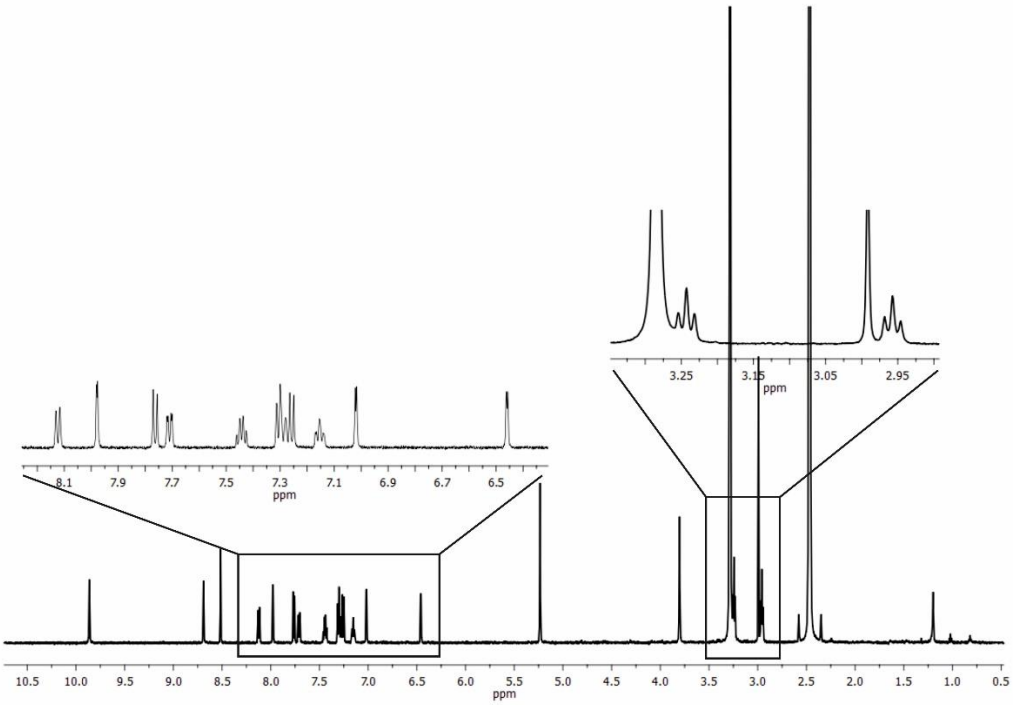


Figure 4.7 - ^{1}H NMR spectrum of lapatinib at pD = 2.0 in a mixture of 30% DMSO and 70% D_2O

To confirm the complex structures, 2D ROESY spectra of the complex were recorded at pD = 2.0. ROESY provides information on through-space interactions between spatially proximate protons (typically within ~5 Å). As an example, the ROESY spectrum of the vandetanib-β-CD complex is shown in Figure 4.8.

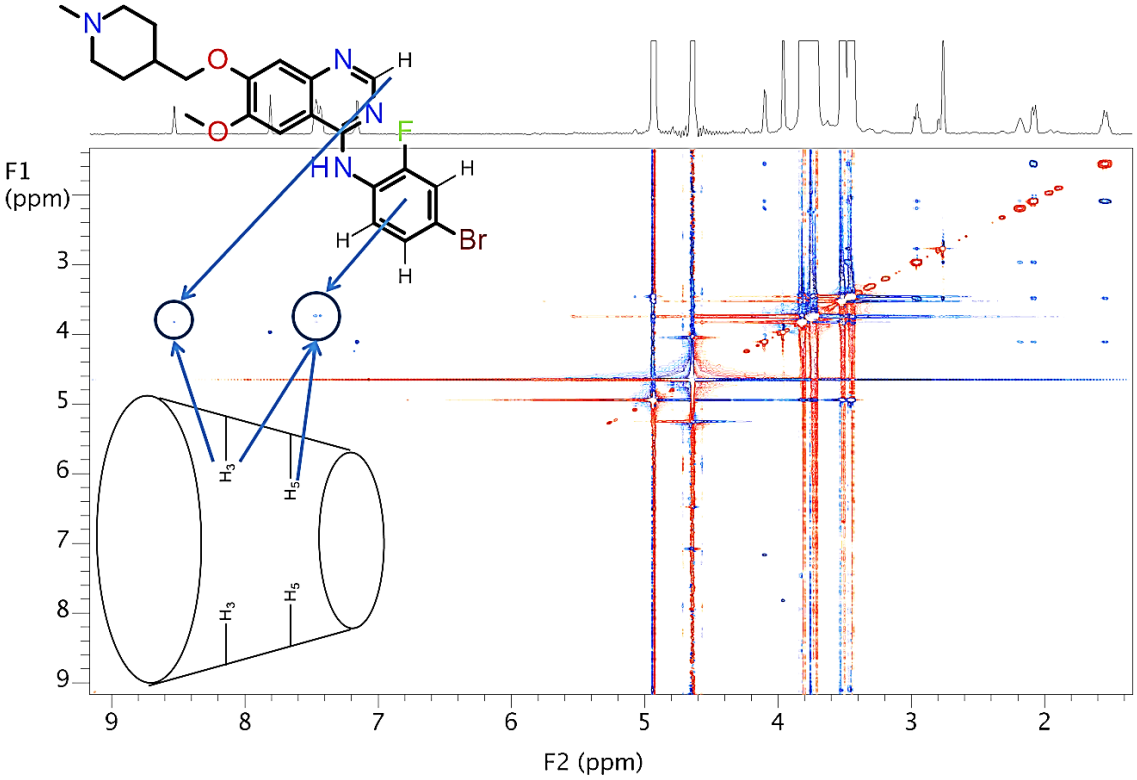


Figure 4.8 - 2D ROESY NMR spectra of vandetanib–β-CD inclusion complex [9].

NMR analysis detected intermolecular interactions between the protons in the bromo-fluorophenyl group of vandetanib and the H^3 and H^5 protons (at 3.62 ppm) in the CD cavity. The ROESY spectrum did not show any cross-peaks involving the H^5 protons of the CD core, which suggests that the bromo-fluorophenyl group of vandetanib predominantly enters the CD core through its wider rim, leading to the formation of an inclusion complex. Similar results were obtained for erlotinib and gefitinib, where the phenyl moiety directly attached to the 4-amino group is accommodated in the CD cavity. In the case of lapatinib, the inclusion complex is formed from the wider rim, where the H^3 protons of CD cross-peaked with the fluorophenyl group.

4.2.4 Molecular modelling

A comprehensive analysis was performed across the four studied TKIs, resulting in eleven selected protonation states for subsequent modelling. For each state, the inhibitor was placed into the β-CD cavity to generate eleven distinct inhibitor–β-CD complexes. The initial orientation within the cavity was guided by ROESY NMR results, which indicated that the more hydrophobic end of each molecule was encapsulated within the CD cavity, as depicted in Figure 4.9. Analogous starting geometries were constructed for all protonation states and subsequently optimized.

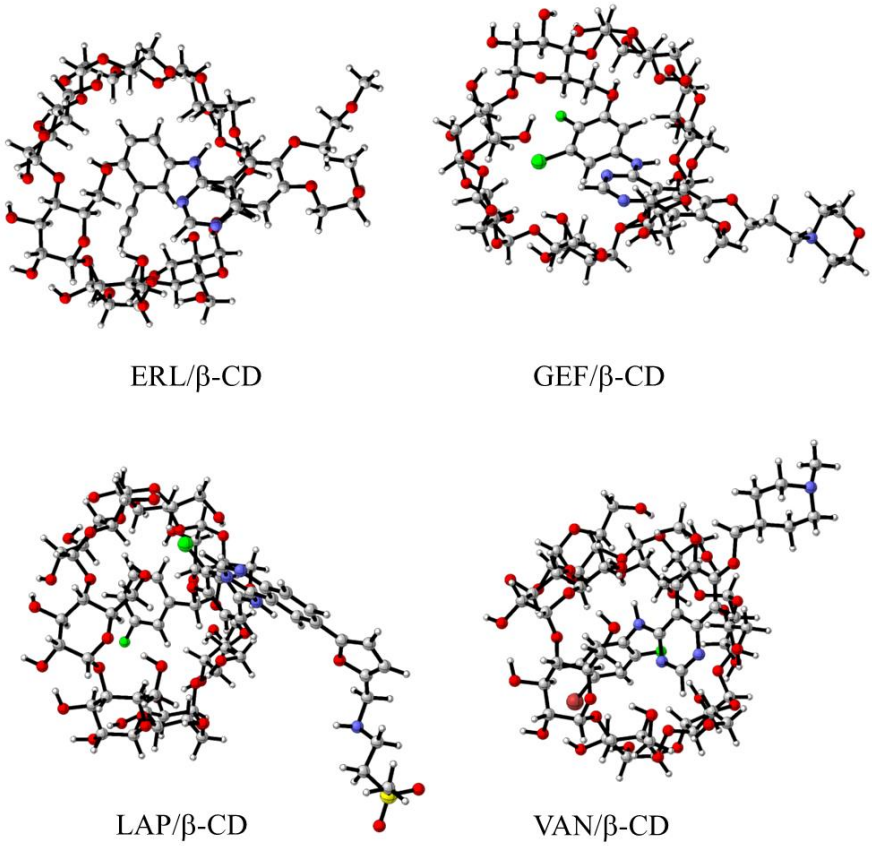


Figure 4.9 - TKI/β-CD complexes optimized at the PM6 level of theory. (ERL – erlotinib, GEF – gefitinib, LAP – lapatinib and VAN – vandetanib) [9].

Table 10. The Gibbs free energies of complex formation were then determined at the PM6 semiempirical level of theory. Calculated relative Gibbs free energies of complex formation (ΔG and ΔΔG, kJ/mol) determined at the PM6 semi-empirical level of theory. The numbered TKI names refer to the optimized protonation states in Table 3 - 6. (ERL – erlotinib, GEF – gefitinib, LAP – lapatinib, and VAN – vandetanib) [9].

Complex	**Charge**	**Δ*G*** (kJ/mol)	**ΔΔ*G*** (kJ/mol)
ERL-01 / β -CD	0	+31.07	0.00
ERL-02 / β -CD	+1	+42.68	+11.61
GEF-01 / β -CD	0	+36.62	0.00
GEF-04 / β -CD	+1	+40.76	+4.14
GEF-05 / β -CD	+2	+46.29	+9.67
LAP-01 / β -CD	0	+48.74	0.00
LAP-02 / β -CD	+1	+39.63	-9.11
LAP-09 / β -CD	+2	+46.25	-2.49
VAN-01 / β -CD	0	+37.63	+0.00
VAN-02 / β -CD	+1	+39.68	+2.05
VAN-04 / β -CD	+2	+41.24	+3.60

4.2.5 Study of tyrosine kinase receptor binding of TKIs

In line with previous findings, molecular docking calculations were performed to investigate how the different protonation states of the TKIs bind to the receptor. Molecular docking calculations (Table 11.) revealed that the quinazoline core exhibits excellent alignment across the docked neutral structures of erlotinib, gefitinib, lapatinib, and vandetanib.

Table 11. Calculated docking scores (DS, kcal/mol) of TKIs with different protonation states docked to tyrosine kinase domain (PDB ID: 4HJO). (ERL – erlotinib, GEF – gefitinib, LAP – lapatinib and VAN – vandetanib) [9].

Complex	**Charge**	**Docking score** (kcal/mol)
ERL/TK	0	-9.543
ERL^{+}/TK	+1	-4.806
GEF/TK	0	-9.109
GEF^{+}/TK	+1	-7.994
GEF^{2+}/TK	+2	-0.833
LAP/TK	0	-12.03
LAP^{+}/TK	+1	-8.018
LAP^{2+}/TK	+2	-2.148
VAN/TK	0	-5.255
VAN^{+}/TK	+1	-5.225
VAN^{2+}/TK	+2	-2.436

In the current study, molecular docking simulations were performed to explore the interactions between various TKIs and the tyrosine kinase domain (PDB ID: 4HJO) in their different protonation states. Specifically, the docking experiments included the

neutral and protonated forms of erlotinib (ERL and ERL^{+}), gefitinib (GEF, GEF^{+}, and GEF^{2+}), lapatinib (LAP, LAP^{+}, and LAP^{2+}), and vandetanib (VAN, VAN^{+}, and VAN^{2+}). Ligand interaction maps were generated to visualize the binding modes, with hydrogen bond interactions between the ligands and the protein residues indicated by purple arrows, pointing from hydrogen bond donors to acceptors (Figure 4.10).

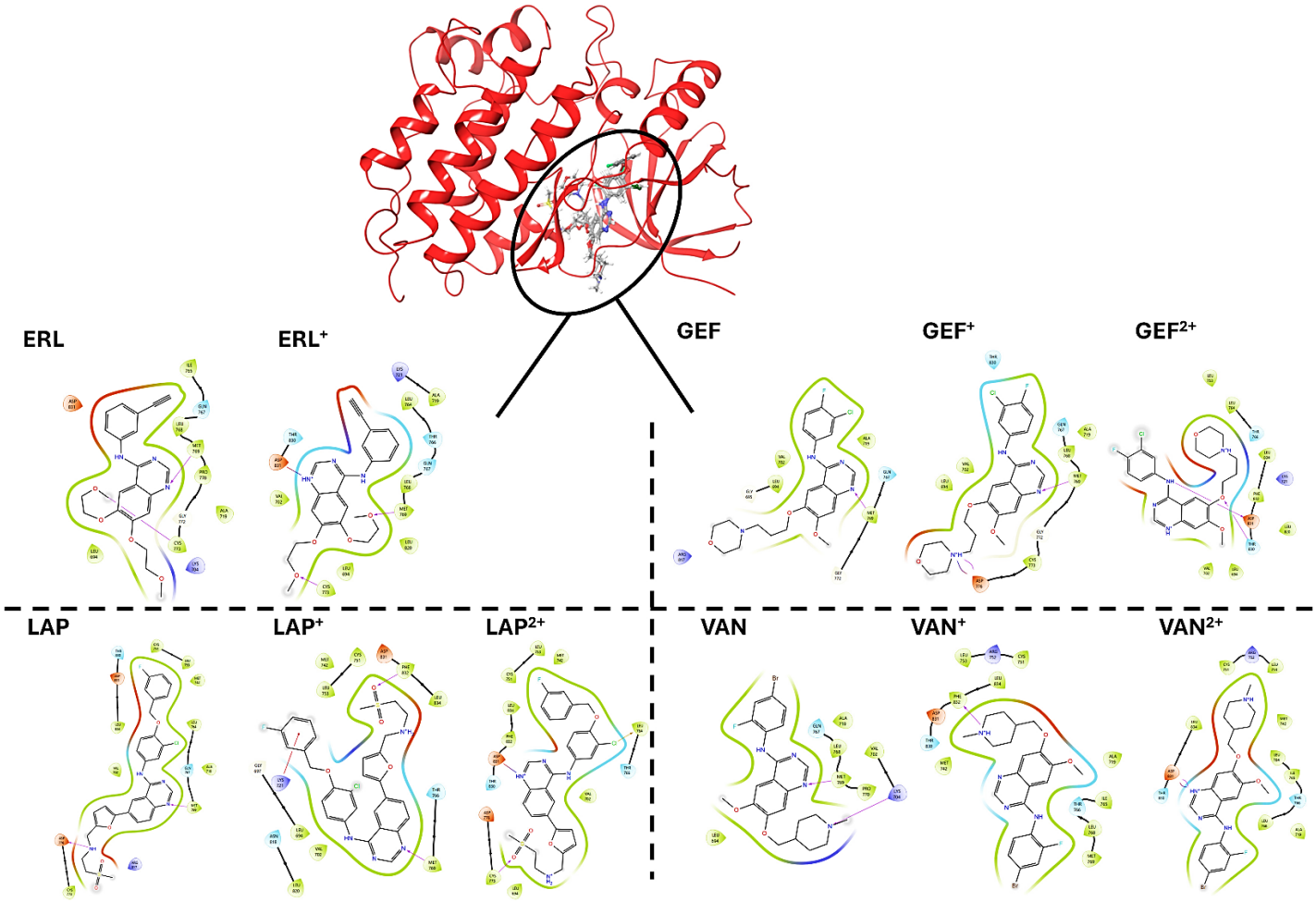


Figure 4.10 - Tyrosine kinase inhibitors docked to the binding site of tyrosine kinase domain (PDB ID: 4HJO). Ligand interaction maps of the docked neutral and protonated erlotinib (ERL and ERL^{+}), gefitinib (GEF, GEF^{+}, and GEF^{2+}), lapatinib (LAP, LAP^{+}, and LAP^{2+}), and vandetanib (VAN, VAN^{+}, and VAN^{2+}) at the binding site of tyrosine kinase domain is also shown. Purple arrows represent hydrogen bonds between the ligand and the protein, and the arrows points from the hydrogen donor to the acceptor [9].

5 DISCUSSION

5.1 Physico-chemical characterization of the studied tyrosine kinase inhibitors

The development of small molecule inhibitors targeting the tyrosine receptor-binding domain of enzymes has emerged as a promising strategy for cancer therapy. Among these inhibitors, compounds with a quinazoline core have received considerable attention due to their high specificity and efficacy. The quinazoline-based TKIs are characterized by a bicyclic core that competitively inhibits the binding of ATP to the tyrosine kinase domain. The activity of these inhibitors is strongly influenced by substitutions on the quinazoline core. The structural modifications represent the most successful compounds of rational drug design to date, aiming to enhance affinity for the ATP binding site, increase selectivity and improve bioavailability. The introduction of the phenyl ring to the quinazoline core resulted in a dramatic increase in its kinase inhibitory activity. However, these compounds have low bioavailability and poor water solubility. To overcome these problems, high polarity side chains (e.g. methoxyethoxy, methylsulfonylethylamino, morpholine or piperidine) were added to the compounds as a final step in the drug design [96].

Assessing the physico-chemical characteristics of pharmaceutical compounds is essential for understanding their pharmacokinetic profiles at the molecular level. Thus, bio-relevant attributes of TKIs, including protonation constants, the octanol/water partition coefficient, and intrinsic solubility were determined (Table 12.).

Table 12. Summarized physico-chemical properties and of TKIs and their bioavailability values. (N/A – not applicable) [9].

	Dissociation constant pK_a			**Lipophilicity** log$P$	**Intrinsic solubility** S_0	**Bioavailability**
	Potentiometric titration	UV-pH titration	NMR-pH titration			
Erlotinib	5.25±0.02	5.39±0.03	5.32±0.06	2.75 ± 0.02	4.91 ± 0.9 µg/ml = 12.5 µM	59%
Gefitinib	**N/A**	**N/A**	5.05±0.02 7.11±0.02	3.65 ± 0.08	86.0 ± 2.53 µg/ml = 192.3 µM	59%
Vandetanib	**N/A**	**N/A**	5.29±0.08 9.11±0.02	4.12 ± 0.13	44.3 ± 0.13 µg/ml = 93.1 µM	**N/A**
Lapatinib	N/A	5.08±0.05 7.72±0.07	N/A	5.65 ± 0.25	0.48 ± 0.12 ng/ml = 210.0 pM	Less than 25%

A comparative evaluation of the protonation constants of erlotinib supports the reliability of each technique. Comparing the different methods provides cross-validation, enhancing both the accuracy and robustness of physicochemical determination. The slight variations observed among the methods reflect their specific sensitivities and experimental conditions, emphasizing the importance of using complementary approaches for a comprehensive understanding. Based on the results obtained, the constant of the single protonatable group of erlotinib was found to be within the error range of 5.32. The pK_{a1} value of quinazoline ring was obtained between 5.0 – 5.3 for all the four molecules. The calculated state penalty values indicate that protonation on the quinazoline core occurs at the para N1-position rather than at the additional N3 nitrogen (Figure 5.1).

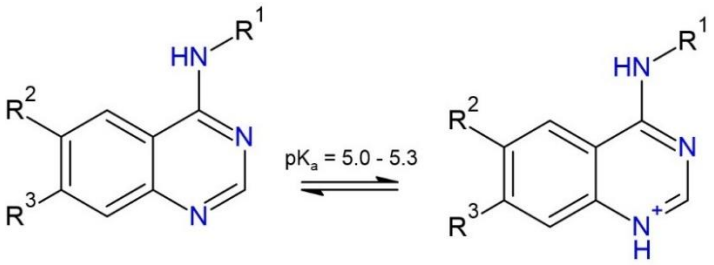


Figure 5.1 - Favored protonation of 4-anilinoquinazoline core calculated by Schrödinger suite [9].

Because the erlotinib study established methodological reliability across techniques, the investigations of gefitinib, vandetanib, and lapatinib proceeded with one optimized method. Since all three techniques (potentiometric titration, UV-pH titration and NMR-pH titration) provided consistent and reliable results for erlotinib, the most practical method was chosen for efficiency. Gefitinib, vandetanib, and lapatinib each contain two protonation centers. Evidently, the aliphatic amino group functions as the stronger basic center than the quinazoline ring. Vandetanib exhibits the most elevated pK_{a2} value at 9.11. In the case of lapatinib and gefitinib, the proximity of an electron-withdrawing group to the aliphatic amine diminishes their pK_{a2} values to 7.72 and 7.11, respectively.

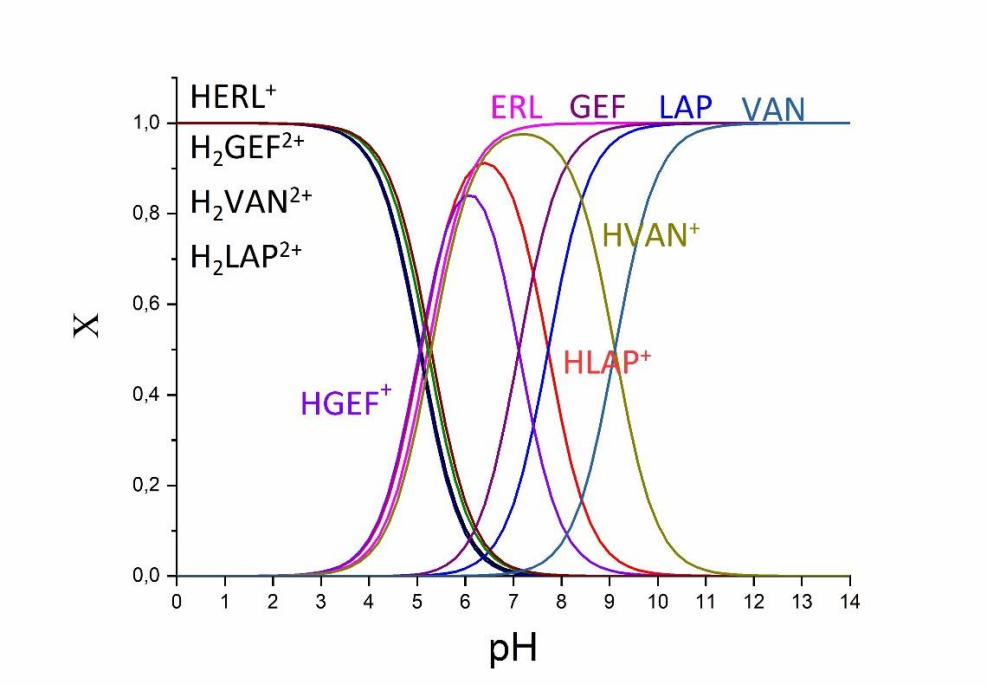


Figure 5.2 - pH-dependent distribution of species of the studied TKIs.
(ERL – erlotinib, GEF – gefitinib, LAP – lapatinib, VAN – vandetanib) [9].

Regarding the pH-dependent distribution of studied TKIs (Figure 5.2) it can be concluded that all four molecules exist predominantly in their (di)cationic form in the highly acidic environment of the stomach, with negligible contributions from the neutral or monocationic forms. This cationic dominance is consistent with the low pH being far below their respective pK_{a1} and pK_{a2} values, leading to full protonation of the molecules. The lack of significant neutral or monocationic forms in this environment suggests that

passive absorption through the stomach lining is minimal or hindered. In the slightly acidic to neutral environment of the intestines, all molecules shift predominantly to their monocationic or neutral form, which is more favorable for passive diffusion across the intestinal epithelium. Below pH 2, over 90% for erlotinib and small percentages of the neutral form persist for gefitinib (~15%), vandetanib (<1%), and lapatinib (~6%), reflecting their respective pK_{a2} values being close to this pH. In the slightly basic environment of the blood, the molecules demonstrate more complex behavior. Erlotinib exists almost entirely in its neutral form (~99.0%), suggesting effective transport across membranes in this state. Gefitinib and lapatinib display a significant proportion of the monocationic form (~32-34%), alongside the neutral form (~66-68%), due to their pK_{a2} being close to blood pH. This dual presence influences their solubility and interactions with plasma proteins. Vandetanib is overwhelmingly monocationic (~97%), with only minor contributions from the neutral form (~3%). Its higher pK_{a2} limits deprotonation at physiological pH.

Lipophilicity results are presented in Table 7. Among the compounds studied, lapatinib exhibited the highest lipophilicity with a log*P* value of 5.65 and erlotinib the lowest with more than 2 log*P* unit lower value. This indicates a broad variability in the lipophilic nature of TKIs across different biological environments, suggesting that even their monoprotonated forms possess the capacity to traverse membranes via passive diffusion. The log*D* value at pH 7.4 for the investigated molecules are the following: 5.16 for lapatinib, 2.40 for vandetanib, 3.47 for gefitinib, and 2.75 for erlotinib. A notable dip in lipophilicity for vandetanib was observed, corresponding to the prevalence of its monocationic form. The substantial lipophilicity of TKIs under physiological conditions implies their potential to permeate the blood-brain barrier and accumulate within the central nervous system, offering a possible therapeutic strategy for treating brain metastases [97].

The obtained solubility results highlight significant variability among the studied TKIs, which has important pharmacokinetic and pharmacodynamic implications. Solubility is a key determinant of oral bioavailability, as it influences the extent of drug dissolution in the gastrointestinal tract, a prerequisite for absorption. Among the TKIs analyzed, gefitinib exhibited the highest intrinsic solubility (86.0 μg/ml), followed by vandetanib and erlotinib, with lapatinib demonstrating the lowest solubility (0.48 ng/ml).

From a pharmacodynamic perspective, solubility plays a critical role in achieving and maintaining therapeutic drug concentrations. Erlotinib and gefitinib achieve an absolute bioavailability of 59%. In contrast, lapatinib, with extremely poor solubility, has a bioavailability of less than 25%, demonstrating the significant limitations associated with low solubility. There are no publicly available data on the bioavailability of vandetanib from human studies. Reliable determination was probably not possible due to high variability, influenced by factors such as its moderate solubility, first-pass metabolism and transporter interactions. The low solubility of lapatinib reflects its inability to dissolve adequately in the gastrointestinal tract, which severely limits its absorption and systemic exposure. To overcome this, lapatinib must be administered in high daily doses of 1250 mg to achieve therapeutic plasma concentrations. This large dosing requirement not only imposes a considerable pill burden on patients but also increases the risk of dose-dependent side effects and interindividual variability in response. To address the solubility challenges identified in this study, CD-based complexation was explored as a strategy to enhance the solubility of these TKIs.

5.2 Characterization of cyclodextrin complexation of tyrosine kinase inhibitors

Establishing the stoichiometry of CD inclusion complexes is a prerequisite for the quantitative interpretation of binding and for the subsequent evaluation of solubility enhancement. CD–drug complexes are typically characterized by 1:1 stoichiometry; however, numerous deviations from this have been reported in the literature [98], particularly when a compound contains multiple lipophilic regions, as is also the case for the compounds investigated in this work. Therefore, we first assessed the predominant host–guest ratio by Job's method of continuous variation, which indicated 1:1 complex formation for all complexes.

Importantly, this conclusion was not based solely on the Job plot results. In the subsequent experiments, the phase-solubility isotherms, the detected cross-peaks during 2D NMR ROESY measurements, and the computational modelling provided convergent and mutually consistent evidence supporting predominant 1:1 stoichiometry, thereby justifying the use of 1:1 binding model for comparing complexation efficiency and for interpreting the solubility-enhancing effects of the selected CD derivatives. Beyond

supporting 1:1 complexation, 2D ROESY NMR provides direct, spatial evidence for inclusion by revealing through-space contacts between CD cavity protons (typically H3 and/or H5) and protons of the guest. In our measurements, the observed intermolecular cross-peaks confirmed that complex formation involves true cavity inclusion rather than nonspecific association, and they also indicated which lipophilic moieties of the TKIs are preferentially accommodated and whether inclusion is more consistent with entry from the wider or narrower rim. This level of structural resolution is critical because stability constants alone do not define the binding geometry: different orientations (or partial inclusion) can yield similar stability values yet lead to markedly different physicochemical behavior and formulation performance. The obtained logK_{stab} values confirm that all four TKIs form thermodynamically stable host–guest complexes with the investigated CDs, and that the complex strength is highly dependent on CD type, with the most pronounced stabilization observed for substituted β-CD derivatives (especially SBE-β-CD). It is widely reported that moderate-to-strong stability constants (often in the range of 10^2–10^4 M^{-1}, depending on the system) are favorable for formulation, as they provide sufficiently stable complexation while maintaining reversibility. Our values fall within or close to this commonly applied range. Therefore, these stability data support the feasibility of CD-based complexation as a formulation-enabling strategy, providing a quantitative basis for selecting the most appropriate CD derivative for further development. The stability constant values are dependent on the ionization state of the guest, that was investigated by molecular modeling techniques between TKIs and β-CD. As we expected, the neutral, non-ionized species form the most stable complex with native β-CD in case of erlotinib, gefitinib and vandetanib. In contrast, for lapatinib, we found no clear correlation between charge and complex stability. This can be explained by the specific characterics of the molecular structure. Lapatinib has a larger hydrophobic unit, and based on structural analysis, the stabilizing hydrogen bond between the molecule's N–H group and the hydroxyl groups of β-CD—which is present in the case of the other inhibitors—cannot form. This hydrogen bond contributes to the stability of the complex in the other systems.

The results of this study also demonstrate the significant impact of CDs on the solubility enhancement of poorly water-soluble drugs, with notable differences in efficacy across the various CD derivatives tested. The data reveal that the choice of CD

plays a critical role in determining the extent of solubility enhancement. SBE-β-CD consistently demonstrated the strongest interactions with the TKIs, as indicated by the high stability constants and exceptional solubility enhancement factors. Its performance was particularly remarkable for lapatinib, achieving a logK_{stab} of 4.33 and a dramatic 183-fold increase in solubility. For the other TKIs, SBE-β-CD also achieved substantial solubility enhancements, including a 23-fold increase for erlotinib, 17-fold for vandetanib, and 34-fold for gefitinib. These results suggest that the sulfobutylether substitution on the β-CD backbone significantly enhances its ability to form stable inclusion complexes with a broad range of poorly soluble drugs. The superior performance of SBE-β-CD can be attributed to its unique physicochemical properties. The introduction of negatively charged sulfobutylether groups increases the hydrophilicity and electrostatic interactions of the CD, which may contribute to stronger drug binding and improved solubility in aqueous environments. Additionally, the modified cavity size of SBE-β-CD appears to be well-suited for accommodating the molecular structures of the tested drugs, particularly lapatinib and gefitinib. These findings highlight the potential of SBE-β-CD as a key excipient for enhancing the solubility and bioavailability of hydrophobic basic drugs, especially those with extremely poor aqueous solubility.

While SBE-β-CD demonstrated the highest efficacy, HP-β-CD and RAMEB also showed strong interactions and substantial solubility enhancements across the four drugs. HP-β-CD, achieved consistent solubility enhancement factors ranging from a 3.1-fold to 4.7-fold increase, making it a viable alternative to SBE-β-CD in scenarios where moderate solubility enhancement is sufficient. Similarly, RAMEB demonstrated notable solubility enhancement for lapatinib (4.5-fold increase) and moderate efficacy for the other TKIs, suggesting that methylation of β-CD improves its binding affinity for certain drug molecules. Both HP-β-CD and RAMEB are widely recognized for their favorable safety profiles and regulatory acceptance, making them practical choices for drug formulations. Their moderate solubility enhancement capabilities make them suitable for drugs that require less drastic modifications to their solubility profiles. Overall, the combined stoichiometric, structural, thermodynamic, and modelling evidence demonstrates that CD complexation—particularly with appropriately substituted β-CD

derivatives—offers a robust, mechanistically well-founded, and highly promising platform for advancing these TKIs toward effective, formulation-ready drug products.

5.3 Evaluation of interactions with the binding domain of tyrosine kinase

The protonation state of both the receptor and the ligand play a pivotal role in determining receptor binding affinity and the accuracy of molecular docking simulations. Ionizable groups within these molecules can undergo protonation or deprotonation during complex formation, leading to pH-dependent binding behaviour. Such protonation state shifts can profoundly influence the binding affinity and binding mode by altering critical intermolecular interactions, including hydrogen bonds, salt bridges, and electrostatic forces, all of which are highly sensitive to the charge state of the interacting molecular partners. As a result, the precise assignment of protonation states is indispensable for the realistic simulation of receptor–ligand interactions. However, this task is inherently challenging due to the dynamic and often poorly defined microenvironments at binding sites, which can significantly impact local protonation equilibria.

Traditional docking protocols often simplify this complexity by assuming fixed protonation states for both the receptor and the ligand, which can lead to inaccuracies in modelling the binding process. An ideal docking approach would involve the simultaneous consideration of all relevant protonation and tautomeric states of the ligand, allowing for a more comprehensive exploration of receptor–ligand interaction dynamics. This approach is particularly critical for TKIs, as their ionization states can significantly affect their binding properties. Docking studies that account for the different protonation states of TKIs not only provide a deeper understanding of the molecular-level interactions between these inhibitors and their target tyrosine kinase domains but also serve as a valuable tool for rational drug design and optimization [99].

The docking results demonstrated that the quinazoline core of the TKIs exhibits excellent alignment across the docked neutral structures of erlotinib, gefitinib, lapatinib, and vandetanib. Key interactions were observed between the ligands and binding site residues, such as MET769 and PHE832, which are critical for stabilizing the receptor–ligand complex. Interestingly, as the charge state of the TKIs increased, the binding modes of the ligands deviated from their positions in the neutral species, except for

monoprotonated gefitinib. Notably, for monoprotonated gefitinib, the core of the ligand maintained the same position as its neutral form, suggesting a unique binding behaviour compared to the other TKIs. In all other cases, the protonated ligands engaged in additional or altered interactions with the protein, leading to significant changes in binding mode. These differences are clearly depicted in the ligand interaction maps (Figure 4.10). Furthermore, all neutral TKI structures were found to interact with MET769, a finding that aligns with previous studies and emphasizes the importance of this residue in the binding mechanism (Figure 4.10) [100]. In terms of docking scores, the neutral TKIs consistently exhibited the most favourable binding, forming the most stable complexes, while the least favourable interactions were observed for the ligands with the highest charge states (Table 11.). Interestingly, the neutral and monoprotonated gefitinib structures showed a greater difference in docking scores (>1 kcal/mol) compared to the neutral and protonated vandetanib pair (0.03 kcal/mol). Structural analysis revealed that despite this difference, the neutral and protonated forms of gefitinib and vandetanib exhibit significant overlap in their binding poses.

In summary, these findings highlight the critical role of protonation states in modulating the binding interactions of TKIs with their target receptors. Accurate modeling of these effects is essential not only for understanding the molecular basis of receptor–ligand recognition but also for guiding the rational design and optimization of TKIs in therapeutic applications.

6 CONCLUSIONS

My first objective was to describe the pharmacokinetic behavior of TKIs at an atomic level by determining the physicochemical properties of four notable TKIs—erlotinib, gefitinib, vandetanib, and lapatinib. As a result of rational drug development, modern TKIs contain more protonatable groups, which can improve the solubility of these molecules. Protonation of the quinazoline ring was identified as a critical factor for efficient receptor binding, and molecular docking studies highlighted the impact of protonation state–dependent interactions on this process. Overall, the physicochemical results confirmed the key pharmacokinetic challenges associated with TKIs, particularly limited bioavailability due to high lipophilicity and low water solubility—a common issue for BCS class II drugs.

CDs can increase the solubility of these active compounds by forming inclusion complexes, which may lead to improved bioavailability. Our in-depth analysis demonstrated that the cavity size of β-CD is particularly well suited for incorporating these molecules. The inclusion complexes formed between the TKIs and β-CD showed a consistent 1:1 stoichiometry, as confirmed by Job plot titration. Furthermore, 2D ROESY NMR spectroscopy and molecular modelling provided atomic-level structural insights into the complexes, contributing to a deeper understanding of TKI pharmacokinetics and receptor binding. Among the modified β-CDs evaluated—randomly methylated, hydroxypropylated, and sulfobutylated β-CDs—sulfobutylated β-CD produced the most pronounced improvement, with up to two orders of magnitude higher solubility.

The outcomes of this study address major drug-development challenges associated with poor water solubility in oncological therapeutics. The biocompatible nature of CD complexes, coupled with their favorable toxicological properties, underscores the importance of continued research in this area. Overall, the results presented in this dissertation contribute to the field of TKI development and provide a quantitative and mechanistic basis for the design of new drug formulations, thereby expanding therapeutic options for cancer patients and advancing oncology pharmacotherapy.

7 SUMMARY

The detailed physicochemical characterization and CD complexation of four key TKIs—erlotinib, gefitinib, vandetanib, and lapatinib—were investigated. A broad set of analytical techniques was applied to study the acid–base properties, lipophilicity, and solubility of these drugs, highlighting low solubility as a fundamental barrier to their bioavailability.

CD complexation emerged as a promising strategy to improve the performance of the studied TKIs. The stoichiometry and stability constants of inclusion complexes formed with native CDs (α-CD, β-CD, γ-CD) and substituted derivatives were characterized using different analytical methods.

Phase-solubility studies demonstrated that CD complexation can substantially enhance the water solubility of the investigated TKIs, with the potential to improve bioavailability. In addition, NMR and molecular modelling were used to examine the stoichiometry and geometry of the complexes, providing mechanistic insights that can support formulation design and inform the further development of TKI-based therapeutics.

8 REFERENCES

1. Arora A, Scholar EM. Role of tyrosine kinase inhibitors in cancer therapy. J Pharmacol Exp Ther. 2005;315(3):971–979. doi:10.1124/jpet.105.084145

2. Sako Y, Minoghchi S, Yanagida T. Single-molecule imaging of EGFR signalling on the surface of living cells. Nat Cell Biol. 2000;2(3):168–172. doi:10.1038/35004044

3. Orton RJ, Sturm OE, Vyshemirsky V, Calder M, Gilbert DR, Kolch W. Computational modelling of the receptor-tyrosine-kinase-activated MAPK pathway. Biochem J. 2005;392(2):249–261. doi:10.1042/BJ20050908

4. Vella F. Molecular biology of the cell: By B Alberts, D Bray, J Lewis, M Raff, K Roberts and J D Watson. pp 1361. Garland Publishing, New York and London. Biochem Educ. 1994;22(3):164–165. doi:10.1016/0307-4412(94)90059-0

5. Vulpetti A, Bosotti R. Sequence and structural analysis of kinase ATP pocket residues. Il Farmaco. 2004;59(10):759–765. doi:10.1016/j.farmac.2004.05.010

6. Silnitsky S, Rubin SJS, Zerihun M, Qvit N. An update on protein kinases as therapeutic targets—Part I: Protein kinase C activation and its role in cancer and cardiovascular diseases. Int J Mol Sci. 2023;24(24):17600. doi:10.3390/ijms242417600

7. Borgo C, D'Amore C, Sarno S, Salvi M, Ruzzene M. Protein kinase CK2: A potential therapeutic target for diverse human diseases. Signal Transduct Target Ther. 2021;6(1):183. doi:10.1038/s41392-021-00567-7

8. Lemmon MA, Schlessinger J. Cell signaling by receptor tyrosine kinases. Cell. 2010;141(7):1117–1134. doi:10.1016/j.cell.2010.06.011

9. Jánoska Á, Szabó ZI, Szőcs L, Fiser B, Tóth G. Physicochemical characterization, cyclodextrin complexation, and protonation state-dependent receptor binding of selected tyrosine kinase inhibitors. J Mol Struct. 2026;1352:144518. doi:10.1016/j.molstruc.2025.144518

10. Salomon DS, Brandt R, Ciardiello F, Normanno N. Epidermal growth factor-related peptides and their receptors in human malignancies. Crit Rev Oncol Hematol. 1995;19(3):183–232. doi:10.1016/1040-8428(94)00144-I

11. Shepherd FA, Rodrigues Pereira J, Ciuleanu T, Tan EH, Hirsh V, Thongprasert S, Campos D, Maoleekoonpiroj S, Smylie M, Martins R, van Kooten M, Dediu M, Findlay B, Tu D, Johnston D, Bezjak A, Clark G, Santabárbara P, Seymour L. Erlotinib in previously treated non-small-cell lung cancer. N Engl J Med. 2005;353(2):123–132. doi:10.1056/NEJMoa050753

12. Moore MJ, Goldstein D, Hamm J, Figer A, Hecht JR, Gallinger S, Au HJ, Murawa P, Walde D, Wolff RA, Campos D, Lim R, Ding K, Clark G, Voskoglou-Nomikos T, Ptasynski M, Parulekar W. Erlotinib plus gemcitabine compared with gemcitabine alone in patients with advanced pancreatic cancer: A phase III trial of the National Cancer Institute of Canada Clinical Trials Group. J Clin Oncol. 2007;25(15):1960–1966. doi:10.1200/JCO.2006.07.9525

13. Roche Registration Limited. Tarceva 25 mg film-coated tablet. EU Summary of Product Characteristics [Internet]. 2010 [cited 2026 May 25]. Available from: https://www.ema.europa.eu/en/documents/product-information/tarceva-epar-product-information_en.pdf

14. Hidalgo M, Siu LL, Nemunaitis J, Rizzo J, Hammond LA, Takimoto C, Eckhardt SG, Tolcher A, Britten CD, Denis L, Ferrante K, Von Hoff DD, Silberman S, Rowinsky EK. Phase I and pharmacologic study of OSI-774, an epidermal growth factor receptor tyrosine kinase inhibitor, in patients with advanced solid malignancies. J Clin Oncol. 2001;19(13):3267–3279. doi:10.1200/JCO.2001.19.13.3267

15. Hynes NE, Lane HA. ERBB receptors and cancer: The complexity of targeted inhibitors. Nat Rev Cancer. 2005;5(5):341–354. doi:10.1038/nrc1609

16. Slamon DJ, Clark GM, Wong SG, Levin WJ, Ullrich A, McGuire WL. Human breast cancer: Correlation of relapse and survival with amplification of the HER-2/neu oncogene. Science. 1979;235(4785):177–182. doi:10.1126/science.3798106

17. Grandis JR, Melhem MF, Gooding WE, Day R, Holst VA, Wagener MM, Drenning SD, Tweardy DJ. Levels of TGF-α and EGFR protein in head and neck squamous cell carcinoma and patient survival. J Natl Cancer Inst. 1998;90(11):824–832. doi:10.1093/jnci/90.11.824

18. U.S. Food and Drug Administration. Pharmacology review and evaluation of Tykerb (lapatinib) [Internet]. Application number: 22-059. Silver Spring (MD): Center for Drug Evaluation and Research; 2007 [cited 2026 May 25]. Available from: https://www.accessdata.fda.gov/drugsatfda_docs/nda/2007/022059s000_PharmR_P1.pdf

19. Koch KM, Reddy NJ, Cohen RB, Lewis NL, Whitehead B, Mackay K, Stead A, Beelen AP, Lewis LD. Effects of food on the relative bioavailability of lapatinib in cancer patients. J Clin Oncol. 2009;27(8):1191–1196. doi:10.1200/JCO.2008.18.3285

20. Sordella R, Bell DW, Haber DA, Settleman J. Gefitinib-sensitizing EGFR mutations in lung cancer activate anti-apoptotic pathways. Science. 2004;305(5687):1163–1167. doi:10.1126/science.1101637

21. Swaisland HC, Smith RP, Laight A, Kerr DJ, Ranson M, Wilder-Smith CH, Duvauchelle T. Single-dose clinical pharmacokinetic studies of gefitinib. Clin Pharmacokinet. 2005;44(11):1165–1177. doi:10.2165/00003088-200544110-00004

22. AstraZeneca AB. Iressa 250 mg film-coated tablets. EU summary of product characteristics [Internet]. 2009 [cited 2026 May 25]. Available from: https://www.ema.europa.eu/en/documents/product-information/iressa-epar-product-information_en.pdf

23. AstraZeneca AB. Caprelsa film-coated tablet. EU summary of product characteristics [Internet]. 2011 [cited 2026 May 25]. Available from: https://www.ema.europa.eu/en/documents/product-information/caprelsa-epar-product-information_en.pdf

24. Martin P, Oliver S, Kennedy SJ, Partridge E, Hutchison M, Clarke D, Giles P. Pharmacokinetics of vandetanib: Three phase I studies in healthy subjects. Clin Ther. 2012;34(1):221–237. doi:10.1016/j.clinthera.2011.11.011

25. Yadav TT, Moin Shaikh G, Kumar MS, Chintamaneni M, YC M. A review on fused pyrimidine systems as EGFR inhibitors and their structure–activity relationship. Front Chem. 2022;10. doi:10.3389/fchem.2022.861288

26. Bjerrum J, Nielsen EJ, Lang S, Rautanen N, Tuhkanen A. Metal ammine formation in aqueous solution. Acta Chem Scand. 1948;2:297–318. doi:10.3891/acta.chem.scand.02-0297

27. Avdeef A. Physicochemical profiling (solubility, permeability and charge state). Curr Top Med Chem. 2001;1(4):277–351. doi:10.2174/1568026013395100

28. Szakács Z. Accurate determination of low pK values by 1H NMR titration. Talanta. 2004;62(4):819–825. doi:10.1016/j.talanta.2003.10.007

29. Avdeef A, Kearney DL, Brown JA, Chemotti AR. Bjerrum plots for the determination of systematic concentration errors in titration data. Anal Chem. 1982;54(13):2322–2326. doi:10.1021/ac00250a041

30. Gran G. Determination of the equivalence point in potentiometric titrations. Part II. Analyst. 1952;77(920):661–671. doi:10.1039/an9527700661

31. Rossotti FJC, Rossotti H. Potentiometric titrations using Gran plots: A textbook omission. J Chem Educ. 1965;42(7):375–378. doi:10.1021/ed042p375

32. Ter Heine R, Fanggiday JC, Lankheet NAG, Beijnen JH, Van Der Westerlaken MML, Staaks GHA, Malingré MM. Erlotinib and pantoprazole: A relevant interaction or not? Br J Clin Pharmacol. 2010;70(6):908–911. doi:10.1111/j.1365-2125.2010.03748.x

33. Avdeef A, Comer JEA, Thomson SJ. pH-metric log P. 3. Glass electrode calibration in methanol-water, applied to pKa determination of water-insoluble substances. Anal Chem. 1993;65(1):42–49. doi:10.1021/ac00049a010

34. Avdeef A, Box KJ, Comer JEA, Gilges M, Hadley M, Hibbert C, Patterson W, Tam KY. pH-metric log P. 11. pKa determination of water-insoluble drugs in organic solvent-water mixtures. J Pharm Biomed Anal. 1999;20(4):631–641. doi:10.1016/S0731-7085(98)00235-0

35. Albert A, Serjeant EP. Determination of ionization constants by spectrophotometry. In: The Determination of Ionization Constants: A Laboratory Manual. Dordrecht: Springer Netherlands; 1984; p. 70–101. doi:10.1007/978-94-009-5548-6_4

36. Rived F, Canals I, Bosch E, Rosés M. Acidity in methanol-water. Anal Chim Acta. 2001;439(2):315–333. doi:10.1016/S0003-2670(01)01046-7

37. Yasuda M. Dissociation constants of some carboxylic acids in mixed aqueous solvents. Bull Chem Soc Jpn. 1959;32(5):429–432. doi:10.1246/bcsj.32.429

38. Shedlovsky T. The behaviour of carboxylic acids in mixed solvents. New York: Pergamon Press. 1962;146–151.

39. Völgyi G, Ruiz R, Box K, Comer J, Bosch E, Takács-Novák K. Potentiometric and spectrophotometric pKa determination of water-insoluble compounds: Validation study in a new cosolvent system. Anal Chim Acta. 2007;583(2):418–428. doi:10.1016/j.aca.2006.10.015

40. Rusu A, Tóth G, Szőcs L, Kökösi J, Kraszni M, Gyéresi Á, Noszál B. Triprotic site-specific acid-base equilibria and related properties of fluoroquinolone antibacterials. J Pharm Biomed Anal. 2012;66:50–57. doi:10.1016/j.jpba.2012.02.024

41. Orgován G, Noszál B. NMR-based determination of pH, free of electrodes and reference compounds. Anal Chem. 2018;90(20):12075–12080. doi:10.1021/acs.analchem.8b02886

42. Govindaraju V, Young K, Maudsley AA. Proton NMR chemical shifts and coupling constants for brain metabolites. NMR Biomed. 2000;13(3):129–153. doi:10.1002/1099-1492(200005)13:3<129::AID-NBM619>3.0.CO;2-V

43. Szakács Z, Hägele G, Tyka R. 1H/31P NMR pH indicator series to eliminate the glass electrode in NMR spectroscopic pKa determinations. Anal Chim Acta. 2004;522(2):247–258. doi:10.1016/j.aca.2004.07.005

44. Moon RB, Richards JH. Determination of intracellular pH by 31P magnetic resonance. J Biol Chem. 1973;248(20):7276–7278. doi:10.1016/S0021-9258(19)43389-9

45. Orgován G, Noszál B. Electrodeless, accurate pH determination in highly basic media using a new set of 1H NMR pH indicators. J Pharm Biomed Anal. 2011;54(5):958–964. doi:10.1016/j.jpba.2010.11.022

46. Wishart DS, Sykes BD. Chemical shifts as a tool for structure determination. Methods Enzymol. 1994;239:363–392. doi:10.1016/S0076-6879(94)39014-2

47. Han GE, Priefer R. A systematic review of various pKa determination techniques. Int J Pharm. 2023;635:122783. doi:10.1016/j.ijpharm.2023.122783

48. Takács-Novák K, Józan M, Hermecz I, Szász G. Lipophilicity of antibacterial fluoroquinolones. Int J Pharm. 1992;79(1–3):89–96. doi:10.1016/0378-5173(92)90099-N

49. Valkó K. Application of high-performance liquid chromatography based measurements of lipophilicity to model biological distribution. J Chromatogr A. 2004;1037(1–2):299–310. doi:10.1016/j.chroma.2003.10.084

50. Mannhold R, Poda GI, Ostermann C, Tetko IV. Calculation of molecular lipophilicity: State-of-the-art and comparison of logP methods on more than 96,000 compounds. J Pharm Sci. 2009;98(3):861–893. doi:10.1002/jps.21494

51. I. Mutton. Fast generic HPLC methods. Separation Methods in Drug Synthesis and Purification. Amsterdam: Elsevier. 2000;73.

52. McNair HM, Miller JM. Basic Gas Chromatography. 2nd ed. Hoboken: Wiley. 2009;135–144.

53. Leo A, Hansch C, Elkins D. Partition coefficients and their uses. Chem Rev. 1971;71(6):525–616. doi:10.1021/cr60274a001

54. Dearden JC, Bresnen GM. The measurement of partition coefficients. Quant Struct-Act Relat. 1988;7(3):133–144. doi:10.1002/qsar.19880070304

55. Könemann H, Zelle R, Busser F, Hammers WE. Determination of log Poct values of chloro-substituted benzenes, toluenes and anilines by high-performance liquid chromatography on ODS-silica. J Chromatogr. 1979;178(2):559–565. doi:10.1016/S0021-9673(00)92516-0

56. Lipinski CA, Lombardo F, Dominy BW, Feeney PJ. Experimental and computational approaches to estimate solubility and permeability in drug discovery and development settings. Adv Drug Deliv Rev. 1997;23(1–3):3–25. doi:10.1016/S0169-409X(96)00423-1

57. Stuart M, Box K. Chasing Equilibrium: Measuring the Intrinsic Solubility of Weak Acids and Bases. Anal Chem. 2005 Feb 1;77(4):983–90. doi:10.1021/ac048767n

58. Crini G. A history of cyclodextrins. Chem Rev. 2014;114(21):10940–10975. doi:10.1021/cr500081p

59. Del Valle EMM. Cyclodextrins and their uses: A review. Process Biochem. 2004;39(9):1033–1046. doi:10.1016/S0032-9592(03)00258-9

60. Loftsson T, Duchene D. Cyclodextrins and their pharmaceutical applications. Int J Pharm. 2007;329(1–2):1–11. doi:10.1016/j.ijpharm.2006.10.044

61. Loftsson T, Brewster ME, Másson M. Role of cyclodextrins in improving oral drug delivery. Am J Drug Deliv. 2004;2(4):261–275. doi:10.2165/00137696-200402040-00006

62. Loftsson T, Jarho P, Másson M, Järvinen T. Cyclodextrins in drug delivery. Expert Opin Drug Deliv. 2005;2(2):335–351. doi:10.1517/17425247.2.1.335

63. Szejtli J. Past, present and future of cyclodextrin research. Pure Appl Chem. 2004;76(10):1825–1845. doi:10.1351/pac200476101825

64. Puskás I, Szente L, Szőcs L, Fenyvesi É. Recent list of cyclodextrin-containing drug products. Period Polytech Chem Eng. 2023;67(1):11–17. doi:10.3311/PPch.21222

65. Stella VJ, Rajewski RA. Cyclodextrins: Their future in drug formulation and delivery. Pharm Res. 1997;14(5):556–567. doi:10.1023/A:1012136608249

66. Loftsson T, Konrádsdóttir F, Másson M. Influence of aqueous diffusion layer on passive drug diffusion from aqueous cyclodextrin solutions through biological membranes. Pharmazie. 2006;61:83–89.

67. Connors KA. The stability of cyclodextrin complexes in solution. Chem Rev. 1997;97(5):1325–1358. doi:10.1021/cr960371r

68. Higuchi T, Connors KA. Phase-solubility techniques. Adv Chem Instrum. 1965;4:117–212.

69. Tóth G, Mohácsi R, Rácz Á, Rusu A, Horváth P, Szente L, Béni S, Noszál B. Equilibrium and structural characterization of ofloxacin-cyclodextrin complexation. J Incl Phenom Macrocycl Chem. 2013;77(1–4):291–300. doi:10.1007/s10847-012-0245-2

70. Casu B, Reggiani M, Gallo GG, Vigevani A. Hydrogen bonding and conformation of glucose and polyglucoses in dimethyl-sulphoxide solution. Tetrahedron. 1966;22(9):3061–3083. doi:10.1016/S0040-4020(01)82286-9

71. Thakkar AL, Demarco PV. Cycloheptaamylose inclusion complexes of barbiturates: Correlation between proton magnetic resonance and solubility studies. J Pharm Sci. 1971;60(4):652–653. doi:10.1002/jps.2600600444

72. Szejtli J. Cyclodextrin technology. Dordrecht: Springer Science+Business Media; 1988;14. doi:10.1007/978-94-015-7797-7.

73. Szabó Z, Ludmerczki R, Fiser B, Noszál B, Tóth G. Chiral separation of rasagiline using sulfobutylether-β-cyclodextrin: Capillary electrophoresis, NMR and molecular modeling study. Electrophoresis. 2019;40(15):1897–1903. doi:10.1002/elps.201800482

74. Szabó ZI, Deme R, Mucsi Z, Rusu A, Mare AD, Fiser B, Toma F, Sipos E, Tóth G. Equilibrium, structural and antibacterial characterization of moxifloxacin-β-cyclodextrin complex. J Mol Struct. 2018;1166:228–236. doi:10.1016/j.molstruc.2018.04.045

75. Schneider HJ, Kramer R, Simova S, Schneider U. Host-guest chemistry. 14. Solvent and salt effects on binding constants of organic substrates in macrocyclic host compounds. A general equation measuring hydrophobic binding contributions. J Am Chem Soc. 1988;110(19):6442–6448. doi:10.1021/ja00227a025

76. Connors KA. Population characteristics of cyclodextrin complex stabilities in aqueous solution. J Pharm Sci. 1995;84(7):843–848. doi:10.1002/jps.2600840712.

77. Neuhaus D, Williamson MP. The nuclear Overhauser effect in structural and conformational analysis. 2nd ed. Weinheim: Wiley-VCH; 2000;619.

78. Hwang TL, Shaka AJ. Cross relaxation without TOCSY: Transverse rotating-frame Overhauser effect spectroscopy. J Am Chem Soc. 1992;114(8):3157–3159. doi:10.1021/ja00034a083

79. Mura P. Analytical techniques for characterization of cyclodextrin complexes in aqueous solution: A review. J Pharm Biomed Anal. 2014;101:238–250. doi:10.1016/j.jpba.2014.02.022

80. Avdeef A, Bucher JJ. Accurate measurements of the concentration of hydrogen ions with a glass electrode: Calibrations using the Prideaux and other universal buffer solutions and a computer-controlled automatic titrator. Anal Chem. 1978;50(14):2137–2142. doi:10.1021/ac50036a045

81. Tam KY, Takács-Novák K. Multi-wavelength spectrophotometric determination of acid dissociation constants: A validation study. Anal Chim Acta. 2001;434(1):157–167. doi:10.1016/S0003-2670(01)00810-8

82. Box KJ, Völgyi G, Baka E, Stuart M, Takács-Novák K, Comer JEA. Equilibrium versus kinetic measurements of aqueous solubility, and the ability of compounds

to supersaturate in solution—a validation study. J Pharm Sci. 2006;95(6):1298–1307. doi:10.1002/jps.20613

83. Hwang TL, Shaka AJ. Water suppression that works. Excitation sculpting using arbitrary wave-forms and pulsed-field gradients. J Magn Reson A. 1995;112(2):275–279. doi:10.1006/jmra.1995.1047

84. MacCarthy P. Simplified experimental route for obtaining Job's curves. Anal Chem. 1978;50(14):2165. doi:10.1021/ac50036a059

85. Park JH, Liu Y, Lemmon MA, Radhakrishnan R. Erlotinib binds both inactive and active conformations of the EGFR tyrosine kinase domain. Biochem J. 2012;448(3):417–423. doi:10.1042/BJ20121513

86. Madhavi Sastry G, Adzhigirey M, Day T, Annabhimoju R, Sherman W. Protein and ligand preparation: Parameters, protocols, and influence on virtual screening enrichments. J Comput Aided Mol Des. 2013;27(3):221–234. doi:10.1007/s10822-013-9644-8

87. Søndergaard CR, Olsson MHM, Rostkowski M, Jensen JH. Improved treatment of ligands and coupling effects in empirical calculation and rationalization of pKa values. J Chem Theory Comput. 2011;7(7):2284–2295. doi:10.1021/ct200133y

88. Harder E, Damm W, Maple J, Wu C, Reboul M, Xiang JY, Wang L, Lupyan D, Dahlgren MK, Knight JL, Kaus JW, Cerutti DS, Krilov G, Jorgensen WL, Abel R, Friesner RA. OPLS3: A force field providing broad coverage of drug-like small molecules and proteins. J Chem Theory Comput. 2016;12(1):281–296. doi:10.1021/acs.jctc.5b00864

89. Friesner RA, Murphy RB, Repasky MP, Frye LL, Greenwood JR, Halgren TA, Sanschagrin PC, Mainz DT. Extra precision Glide: Docking and scoring incorporating a model of hydrophobic enclosure for protein-ligand complexes. J Med Chem. 2006;49(21):6177–6196. doi:10.1021/jm051256o

90. Friesner RA, Banks JL, Murphy RB, Halgren TA, Klicic JJ, Mainz DT, Repasky MP, Knoll EH, Shelley M, Perry JK, Shaw DE, Francis P, Shenkin PS. Glide: A new approach for rapid, accurate docking and scoring. 1. Method and assessment

of docking accuracy. J Med Chem. 2004;47(7):1739–1749. doi:10.1021/jm0306430

91. Barone V, Cossi M. Quantum calculation of molecular energies and energy gradients in solution by a conductor solvent model. J Phys Chem A. 1998;102(11):1995–2001. doi:10.1021/jp9716997

92. Cossi M, Rega N, Scalmani G, Barone V. Energies, structures, and electronic properties of molecules in solution with the C-PCM solvation model. J Comput Chem. 2003;24(6):669–681. doi:10.1002/jcc.10189

93. Tóth G, Jánoska Á, Szabó ZI, Völgyi G, Orgován G, Szente L, Noszál B. Physicochemical characterisation and cyclodextrin complexation of erlotinib. Supramol Chem. 2016;28(7–8):656–664. doi:10.1080/10610278.2015.1117083

94. Tóth G, Jánoska Á, Völgyi G, Szabó ZI, Orgován G, Mirzahosseini A, Noszál B. Physicochemical characterization and cyclodextrin complexation of the anticancer drug lapatinib. J Chem. 2017:4537632. doi:10.1155/2017/4537632

95. Larsen KL, Zimmermann W. Analysis and characterisation of cyclodextrins and their inclusion complexes by affinity capillary electrophoresis. J Chromatogr A. 1999;836(1):3–14. doi:10.1016/S0021-9673(99)00091-6

96. Wu P, Nielsen TE, Clausen MH. FDA-approved small-molecule kinase inhibitors. Trends Pharmacol Sci. 2015;36(7):422–439. doi:10.1016/j.tips.2015.04.005

97. Namba Y, Kijima T, Yokota S, Niinaka M, Kawamura S, Iwasaki T, Takeda Y, Kimura H, Okada T, Yamaguchi T, Nakagawa M, Okumura Y, Maeda H, Ito M. Gefitinib in patients with brain metastases from non-small-cell lung cancer: Review of 15 clinical cases. Clin Lung Cancer. 2004;6(2):123–128. doi:10.3816/CLC.2004.n.026

98. Dandawate PR, Vyas A, Ahmad A, Banerjee S, Deshpande J, Swamy KV, Jamadar A, Dumhe-Klaire AC, Padhye S, Sarkar FH. Inclusion complex of novel curcumin analogue CDF and β-cyclodextrin (1:2) and its enhanced in vivo anticancer activity against pancreatic cancer. Pharm Res. 2012;29(7):1775–1786. doi:10.1007/s11095-012-0700-1

99. Petukh M, Stefl S, Alexov E. The role of protonation states in ligand-receptor recognition and binding. Curr Pharm Des. 2013;19(23):4182–4190. doi:10.2174/1381612811319230004

100. Lv PC, Li DD, Li QS, Lu X, Xiao ZP, Zhu HL. Synthesis, molecular docking and evaluation of thiazolyl-pyrazoline derivatives as EGFR TK inhibitors and potential anticancer agents. Bioorg Med Chem Lett. 2011;21(18):5374–5377. doi:10.1016/j.bmcl.2011.07.010

9 BIBLIOGRAPHY OF THE CANDIDATE'S PUBLICATIONS

9.1 Publication relevant to the dissertation

I. Jánoska Á, Szabó ZI, Szőcs L, Fiser B, Tóth G. Physicochemical characterization, cyclodextrin complexation, and protonation state-dependent receptor binding of selected tyrosine kinase inhibitors. J Mol Struct. 2026 Feb;1352:144518.

II. Tóth G*, Jánoska Á*, Szabó ZI, Völgyi G, Orgován G, Szente L, Noszál B. Physicochemical characterisation and cyclodextrin complexation of erlotinib. Supramol Chem. 2016 Aug 2;28(7–8):656–64.

III. Tóth G*, Jánoska Á*, Völgyi G, Szabó ZI, Orgován G, Mirzahosseini A, Noszál B. Physicochemical Characterization and Cyclodextrin Complexation of the Anticancer Drug Lapatinib. J Chem. 2017;2017:1–9.
*Contributed equally to this work

9.2 Other, not related publications

IV. Szabó Z, Szőcs L, Horváth P, Komjáti B, Nagy J, Jánoska Á, Muntean D, Noszál B, Tóth G. Liquid chromatography with mass spectrometry enantioseparation of pomalidomide on cyclodextrin-bonded chiral stationary phases and the elucidation of the chiral recognition mechanisms by NMR spectroscopy and molecular modeling. J Sep Sci. 2016 Aug 6;39(15):2941–9.

10 ACKNOWLEDGEMENTS

I extend my deepest gratitude to my instructor and mentor, Gergő Tóth, whose guidance and unwavering support have been the cornerstone of my academic journey. His invaluable insights and encouragement have been instrumental in my success. I am also immensely thankful to Gergely Völgyi for his expertise and assistance in solubility studies and measurement techniques, which were pivotal in the completion of my research. My appreciation extends to Gábor Orgován and Arash Mirzahosseini, for their advice in NMR spectroscopy and their role as a supervisor, which have greatly enriched my scientific understanding. Special thanks are due to Levente Szőcs from Cyclolab Ltd., for his contributions to my research, providing both valuable insights into cyclodextrins and the necessary materials for my measurements. Furthermore, I express my gratitude to Béla Fiser from the University of Miskolc, whose expertise in molecular modelling has significantly enhanced the scientific rigor of my work. The steadfast support of Gergő Tóth have been essential in enabling me to resume and conclude my PhD studies after a seven-year hiatus. This accomplishment is a testament to the collective effort and dedication of those who have contributed to my professional journey. While my academic pursuits have been a primary focus, my family's understanding and support have been a backdrop to this journey. A special mention goes to my wife, whose patience, unwavering belief in me, and sacrifices have made it possible for me to pursue and achieve this milestone. This dissertation is a culmination of collective wisdom and guidance, and I am thankful to everyone who has played a role in bringing it to fruition.